Modern Theory of Nuclear Forces

E. Epelbaum*

Forschungszentrum Jülich, Institut für Kernphysik (IKP-3) and Jülich Center for Hadron Physics, D-52425 Jülich, Germany and
Helmholtz-Institut für Strahlen- und Kernphysik (Theorie) and Bethe Center for Theoretical Physics, Universität Bonn, D-53115 Bonn, Germany

H.-W. Hammer†

Helmholtz-Institut für Strahlen- und Kernphysik (Theorie) and Bethe Center for Theoretical Physics, Universität Bonn, D-53115 Bonn, Germany

Ulf-G. Meißner‡

Helmholtz-Institut für Strahlen- und Kernphysik (Theorie) and Bethe Center for Theoretical Physics, Universität Bonn, D-53115 Bonn, Germany and
Forschungszentrum Jülich, Institut für Kernphysik (IKP-3) and Jülich Center for Hadron Physics, D-52425 Jülich, Germany

Effective field theory allows for a systematic and model-independent derivation of the forces between nucleons in harmony with the symmetries of Quantum Chromodynamics. We review the foundations of this approach and discuss its application for light nuclei at various resolution scales. The extension of this approach to many-body systems is briefly sketched.

Commissioned article for *Reviews of Modern Physics*

Contents

*Electronic address: e.epelbaum@fz-juelich.de
†Electronic address: hammer@itkp.uni-bonn.de
‡Electronic address: meissner@itkp.uni-bonn.de

I. QCD AND NUCLEAR FORCES

Within the Standard Model of particle physics, the strong interactions are described by Quantum Chromodynmics (QCD). QCD is a fascinating theory with many intriguing manifestations. Its structure and interactions are governed by a local non-abelian gauge symmetry, namely $\mathrm{SU(3)_{color}}$. Its fundamental degrees of freedom, the quarks (the matter fields) and gluons (the force carriers), have never been observed in isolation (confinement). The strong coupling constant α_S exhibits a very pronounced running and is of order one in the typical energy scales of nuclear physics. The bound states made from the basic constituents are the hadrons, the strongly interacting particles. The particle spectrum shows certain regularities that can be traced back to the flavor symmetries related to the fermions building up these states. More precisely, there are six quark flavors. These can be grouped into two very different sectors. While the light quarks (u, d, s) are almost massless and thus have to be treated relativistically, bound states made from heavy quarks allow for a precise non-relativistic treatment. In what follows, we will only consider the light quarks at low energies, where perturbation theory in α_S is inapplicable (this regime is frequently called "strong QCD"). A further manifestation of strong QCD is the appearance of nuclei, shallow bound states composed of protons, neutrons, pions or strange particles like hyperons. The resulting nuclear forces that are responsible for the nuclear binding are residual color forces, much like the van der Waals forces between neutral molecules. It is the aim of this article to provide the link between QCD and its symmetries, in particular the spontaneously and explicitely

broken chiral symmetry, and the nuclear forces which will allow to put nuclear physics on firm theoretical grounds and also gives rise to a very accurate calculational scheme for nuclear forces and the properties of nuclei.

This review is organized as follows: In this section, we briefly discuss some of the concepts underlying the chiral effective field theory of the nuclear forces and make contact to ab initio lattice simulations of two-baryon systems as well as to more phenomenological approaches. Sec. II deals with the foundations and applications of nuclear EFT and should be considered the central piece of this review. In particular, tests of these forces in few-nucleon systems are discussed. Attempts to tackle nuclear matter and finite nuclei are considered in sec. III. We end with a short summary and outlook.

A. Chiral symmetry

First, we must discuss chiral symmetry in the context of QCD. Chromodynamics is a non-abelian $SU(3)_{\rm color}$ gauge theory with $N_f = 6$ flavors of quarks, three of them being light (u, d, s) and the other three heavy (c, b, t). Here, light and heavy refers to a typical hadronic scale of about 1 GeV. In what follows, we consider light quarks only (the heavy quarks are to be considered as decoupled). The QCD Lagrangian reads

$$\begin{aligned} \mathcal{L}_{\rm QCD} &= -\frac{1}{2g^2}{\rm Tr}\,(G_{\mu\nu}G^{\mu\nu}) + \bar{q}\,i\gamma^\mu D_\mu\,q - \bar{q}\mathcal{M}\,q \\ &= \mathcal{L}^0_{\rm QCD} - \bar{q}\mathcal{M}\,q\ , \end{aligned} \tag{1.1}$$

where we have absorbed the gauge coupling in the definition of the gluon field and color indices are suppressed. The three-component vector q collects the quark fields, $q^T(x) = (u(s), d(x), s(x))$. As far as the strong interactions are concerned, the different quarks u, d, s have identical properties, except for their masses. The quark masses are free parameters in QCD - the theory can be formulated for any value of the quark masses. In fact, light quark QCD can be well approximated by a fictitious world of massless quarks, denoted $\mathcal{L}^0_{\rm QCD}$ in Eq. (1.1). Remarkably, this theory contains no adjustable parameter - the gauge coupling g merely sets the scale for the renormalization group invariant scale $\Lambda_{\rm QCD}$. Furthermore, in the massless world left- and right-handed quarks are completely decoupled. The Lagrangian of massless QCD is invariant under separate unitary global transformations of the left- and right-hand quark fields, the so-called *chiral rotations*, $q_I \to V_I q_I$, $V_I \in U(3)$, $I = L, R$, leading to $3^2 = 9$ conserved left- and 9 conserved right-handed currents by virtue of Noether's theorem. These can be expressed in terms of vector $(V = L+R)$ and axial-vector $(A = L - R)$ currents

$$\begin{aligned} V_0^\mu &= \bar{q}\,\gamma^\mu\,q\ , \quad V_a^\mu = \bar{q}\,\gamma^\mu\frac{\lambda_a}{2}\,q\ , \\ A_0^\mu &= \bar{q}\,\gamma^\mu\gamma_5\,q\ , \quad A_a^\mu = \bar{q}\,\gamma^\mu\gamma_5\frac{\lambda_a}{2}\,q\ , \end{aligned} \tag{1.2}$$

Here, $a = 1, \ldots 8$, and the λ_a are Gell-Mann's $SU(3)$ flavor matrices. The singlet axial current is anomalous, and thus not conserved. The actual symmetry group of massless QCD is generated by the charges of the conserved currents, it is $G_0 = SU(3)_R \times SU(3)_L \times U(1)_V$. The $U(1)_V$ subgroup of G_0 generates conserved baryon number since the isosinglet vector current counts the number of quarks minus antiquarks in a hadron. The remaining group $SU(3)_R \times SU(3)_L$ is often referred to as chiral $SU(3)$. Note that one also considers the light u and d quarks only (with the strange quark mass fixed at its physical value), in that case, one speaks of chiral $SU(2)$ and must replace the generators in Eq. (1.2) by the Pauli-matrices. Let us mention that QCD is also invariant under the discrete symmetries of parity (P), charge conjugation (C) and time reversal (T). Although interesting in itself, we do not consider strong CP violation and the related θ-term in what follows, see e.g. (1).

The chiral symmetry is a symmetry of the Lagrangian of QCD but not of the ground state or the particle spectrum – to describe the strong interactions in nature, it is crucial that chiral symmetry is spontaneously broken. This can be most easily seen from the fact that hadrons do not appear in parity doublets. If chiral symmetry were exact, from any hadron one could generate by virtue of an axial transformation another state of exactly the same quantum numbers except of opposite parity. The spontaneous symmetry breaking leads to the formation of a quark condensate in the vacuum $\langle 0|\bar{q}q|0\rangle = \langle 0|\bar{q}_L q_R + \bar{q}_R q_L|0\rangle$, thus connecting the left- with the right-handed quarks. In the absence of quark masses this expectation value is flavor-independent: $\langle 0|\bar{u}u|0\rangle = \langle 0|\bar{d}d|0\rangle = \langle 0|\bar{q}q|0\rangle$. More precisely, the vacuum is only invariant under the subgroup of vector rotations times the baryon number current, $H_0 = SU(3)_V \times U(1)_V$. This is the generally accepted picture that is supported by general arguments (2) as well as lattice simulations of QCD (for a recent study, see (3)). In fact, the vacuum expectation value of the quark condensate is only one of the many possible order parameters characterizing the spontaneous symmetry violation - all operators that share the invariance properties of the vacuum qualify as order parameters. The quark condensate nevertheless enjoys a special role, it can be shown to be related to the density of small eigenvalues of the QCD Dirac operator (see (4) and more recent discussions in (5; 6)), $\lim_{\mathcal{M}\to 0}\langle 0|\bar{q}q|0\rangle = -\pi\,\rho(0)$. For free fields, $\rho(\lambda) \sim \lambda^3$ near $\lambda = 0$. Only if the eigenvalues accumulate near zero, one obtains a non-vanishing condensate. This scenario is indeed supported by lattice simulations and many model studies involving topological objects like instantons or monopoles.

Before discussing the implications of spontaneous symmetry breaking for QCD, we briefly remind the reader of Goldstone's theorem (7; 8): to every generator of a spontaneously broken symmetry corresponds a massless excitation of the vacuum. These states are the *Goldstone bosons*, collectively denoted as pions $\pi(x)$ in what

follows. Through the corresponding symmetry current the Goldstone bosons couple directly to the vacuum,

$$\langle 0|A^0(0)|\pi\rangle \neq 0 \ . \tag{1.3}$$

In fact, the non-vanishing of this matrix element is a *necessary and sufficient* condition for spontaneous symmetry breaking. In QCD, we have eight (three) Goldstone bosons for $SU(3)$ ($SU(2)$) with spin zero and negative parity – the latter property is a consequence that these Goldstone bosons are generated by applying the axial charges on the vacuum. The dimensionful scale associated with the matrix element Eq. (1.3) is the pion decay constant (in the chiral limit)

$$\langle 0|A^a_\mu(0)|\pi^b(p)\rangle = i\delta^{ab}Fp_\mu \ , \tag{1.4}$$

which is a fundamental mass scale of low-energy QCD. In the world of massless quarks, the value of F differs from the physical value by terms proportional to the quark masses, to be introduced later, $F_\pi = F[1+\mathcal{O}(\mathcal{M})]$. The physical value of F_π is 92.4 MeV, determined from pion decay, $\pi \to \nu\mu$.

Of course, in QCD the quark masses are not exactly zero. The quark mass term leads to the so-called *explicit chiral symmetry breaking*. Consequently, the vector and axial-vector currents are no longer conserved (with the exception of the baryon number current)

$$\partial_\mu V^\mu_a = \frac{1}{2}i\bar{q}\,[\mathcal{M},\lambda_a]\,q \ , \quad \partial_\mu A^\mu_a = \frac{1}{2}i\bar{q}\,\{\mathcal{M},\lambda_a\}\,\gamma_5\,q \ . \tag{1.5}$$

However, the consequences of the spontaneous symmetry violation can still be analyzed systematically because the quark masses are *small*. QCD possesses what is called an approximate chiral symmetry. In that case, the mass spectrum of the unperturbed Hamiltonian and the one including the quark masses can not be significantly different. Stated differently, the effects of the explicit symmetry breaking can be analyzed in perturbation theory. As a consequence, QCD has a remarkable mass gap - the pions (and, to a lesser extent, the kaons and the eta) are much lighter than all other hadrons. To be more specific, consider chiral $SU(2)$. The second formula of Eq. (1.5) is nothing but a Ward-identity (WI) that relates the axial current $A^\mu = \bar{d}\gamma^\mu\gamma_5 u$ with the pseudoscalar density $P = \bar{d}i\gamma_5 u$,

$$\partial_\mu A^\mu = (m_u + m_d)\,P \ . \tag{1.6}$$

Taking on-shell pion matrix elements of this WI, one arrives at

$$M^2_\pi = (m_u+m_d)\frac{G_\pi}{F_\pi} \ , \tag{1.7}$$

where the coupling G_π is given by $\langle 0|P(0)|\pi(p)\rangle = G_\pi$. This equation leads to some intriguing consequences: In the chiral limit, the pion mass is exactly zero - in accordance with Goldstone's theorem. More precisely, the ratio G_π/F_π is a constant in the chiral limit and the pion mass grows as $\sqrt{m_u+m_d}$ if the quark masses are turned on.

There is even further symmetry related to the quark mass term. It is observed that hadrons appear in isospin multiplets, characterized by very tiny splittings of the order of a few MeV. These are generated by the small quark mass difference $m_u - m_d$ and also by electromagnetic effects of the same size (with the notable exception of the charged to neutral pion mass difference that is almost entirely of electromagnetic origin). This can be made more precise: For $m_u = m_d$, QCD is invariant under $SU(2)$ isospin transformations: $q \to q' = Uq$, with U a unitary matrix. In this limit, up and down quarks can not be disentangled as far as the strong interactions are concerned. Rewriting of the QCD quark mass term allows to make the strong isospin violation explicit:

$$\begin{aligned}\mathcal{H}^{\rm SB}_{\rm QCD} &= m_u\,\bar{u}u + m_d\,\bar{d}d \\ &= \frac{m_u+m_d}{2}(\bar{u}u+\bar{d}d) + \frac{m_u-m_d}{2}(\bar{u}u-\bar{d}d) \ ,\end{aligned} \tag{1.8}$$

where the first (second) term is an isoscalar (isovector). Extending these considerations to $SU(3)$, one arrives at the eighfold way of Gell-Mann and Ne'eman that played a decisive role in our understanding of the quark structure of the hadrons. The $SU(3)$ flavor symmetry is also an approximate one, but the breaking is much stronger than it is the case for isospin. From this, one can directly infer that the quark mass difference $m_s - m_d$ must be much bigger than $m_d - m_u$.

The consequences of these broken symmetries can be analyzed systematically in a suitably tailored effective field theory (EFT), as discussed in more detail below. At this point, it is important to stress that the chiral symmetry of QCD plays a crucial role in determining the longest ranged parts of the nuclear force, which, as we will show, is given by Goldstone boson exchange between two and more nucleons. This was already stressed long ago, see e.g (9) (and references therein) but only with the powerful machinery of chiral effective field theory this connection could be worked out model-independently, as we will show in what follows.

B. Scales in nuclear physics

To appreciate the complexity related to a theoretical description of the nuclear forces, it is most instructive to briefly discuss the pertinent scales arising in this problem. This can most easily be visualized by looking at the phenomenological central potential between two nucleons, as it appears e.g. in meson-theoretical approaches to the nuclear force, see Fig. 1. The longest range part of the interaction is the one-pion exchange (OPE) that is firmly rooted in QCD's chiral symmetry. Thus, the corresponding natural scale of the nuclear force problem is the Compton wavelength of the pion

$$\lambda_\pi = 1/M_\pi \simeq 1.5\,{\rm fm} \ , \tag{1.9}$$

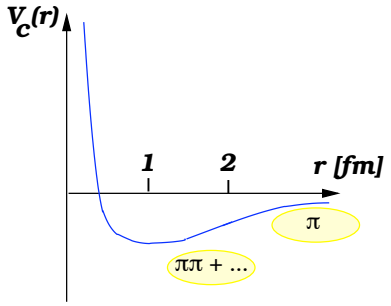

FIG. 1 Schematic plot of the central nucleon-nucleon potential. The longest range contribution is the one-pion-exchange, the intermediate range attraction is described by two-pion exchanges and other shorter ranged contributions. At even shorter distances, the NN interaction is strongly repulsive.

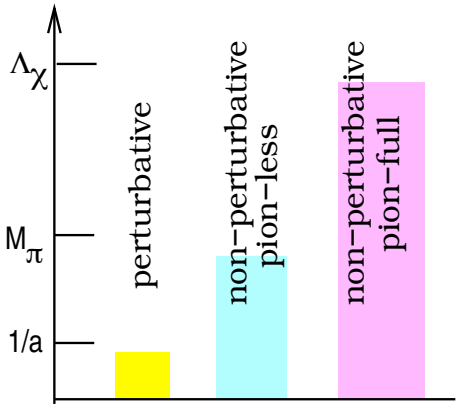

FIG. 2 Scales in the two-nucleon problem and the range of validity of the corresponding EFTs as explained in the text. Here Λ_χ is the hard scale related to spontaneous chiral symmetry breaking, with $\Lambda_\chi \simeq M_\rho$, with $M_\rho = 770\,\mathrm{MeV}$ the mass of the rho meson.

where $M_\pi = 139.57\,\mathrm{MeV}$ is the charged pion mass. The central intermediate range attraction is given by 2π exchange (and shorter ranged physics). Finally, the wave-functions of two nucleons do not like to overlap, which is reflected in a short-range repulsion that can e.g. be modelled by vector meson exchange. From such considerations, one would naively expect to be able to describe nuclear binding in terms of energy scales of the order of the pion mass. However, the true binding energies of the nuclei are given by much smaller energy scales, between 1 to 9 MeV per nucleon. Another measure for the shallow nuclear binding is the so called binding-momentum γ. In the deuteron, $\gamma = \sqrt{mB_D} \simeq 45\,\mathrm{MeV} \ll M_\pi$, with $m = 938.2\,\mathrm{MeV}$ the nucleon mass and $B_D = 2.224\,\mathrm{MeV}$ the deuteron binding energy. The small value of γ signals the appearance of energy/momentum scales much below the pion mass. The most dramatic reflection of the complexity of the nuclear force problem are the values of the S-wave neutron-proton scattering lengths,

$$|a(^1S_0)| = 23.8\,\mathrm{fm} \gg 1/M_\pi\,,\;\; a(^3S_1) = 5.4\,\mathrm{fm} \gg 1/M_\pi\,. \tag{1.10}$$

Thus, to properly set up an effective field theory for the forces between two (or more) nucleons, it is mandatory to deal with these very different energy scales. If one were to treat the large S-wave scattering lengths perturbatively, the range of the corresponding EFT would be restricted to momenta below $p_{\max} \sim 1/|a(^1S_0)| \simeq 8\,\mathrm{MeV}$. To overcome this barrier, one must generate the small binding energy scales by a non-perturbative resummation. This can e.g. be done in a theory without explicit pion degrees of freedom, the so-called pion-less EFT. In such an approach, the limiting hard scale is the pion mass. To go further, one must include the pions explicitely, as it is done in the pion-full or chiral nuclear EFT. The relation between these different approaches is schematically displayed in Fig. 2. A different and more formal argument that shows the breakdown of a perturbative treatment of the EFT with two or more nucleons is related to the pinch singularities in the two-pion exchange diagram in the static limit as will be discussed later in the context of the explicit construction of the chiral nuclear EFT.

In addition, if one extends the considerations to heavier nuclei or even nuclear matter, the many-body system exhibits yet another scale, the Fermi momentum k_F, with $k_F \simeq 2M_\pi$ at nuclear matter saturation density. This new scale must be included in a properly modified EFT for the nuclear many-body problem which is not a straightforward exercise as we will show below. It is therefore not astonishing that the theory for heavier nuclei is still in a much less developed stage that the one for the few-nucleon problem. These issues will be taken up in Sec. III.

For more extended discussions of scales in the nuclear force problem and in nuclei, we refer to (10–13).

C. Conventional approaches to the nuclear force problem

Before discussing the application of the effective field theory approach to the nuclear force problem, let us make a few comments on the highly successful conventional approaches. First, we consider the two-nucleon case. Historically, meson field theory and dispersion relations have laid the foundations for the construction of a two-nucleon potential. All these approaches incorporate the long-range one-pion exchange as proposed by Yukawa in 1935 (14) which nowadays is firmly rooted in QCD. Dispersion relations can be used to construct the two-pion exchange contribution to the nuclear force as pioneered at Paris (15) and Stony Brook (16). For a review, see e.g. (17). In the 1990ties, the so-called high-precision potentials have been developed that fit the large basis of pp and np elastic scattering data with a χ^2/datum $\simeq 1$. One of these is the so-called CD-Bonn potential (18) (which was developed at Moscow, Idaho). Besides one-pion, ρ and ω vector-meson exchanges, it contains two scalar–isoscalar mesons in each partial wave up to angular momentum

$J = 5$ with the mass and coupling constant of the second σ fine-tuned in any partial wave. The hadronic vertices are regulated with form factors with cut-offs ranging from 1.3 to 1.7 GeV. Similarly, in the Nijmegen I,II potentials one–pion exchange is supplemented by heavy boson exchanges with adjustable parameters which are fitted for all (low) partial waves separately (19). The Argonne V18 (AV18) potential starts from a very general operator structure in coordinate space and has fit functions for all these various operators (20). While these various potentials give an accurate representation of the nucleon-nucleon phase shifts and of most deuteron properties, the situation becomes much less satisfactory when it comes to the much smaller but necessary three-nucleon forces. Such three-body forces are needed to describe the nuclear binding energies and levels, as most systematically shown by the Urbana-Argonne group (21). Systematic studies of the dynamics and reactions of systems with three or four-nucleons further sharpen the case for the necessity of including three-nucleon forces (3NFs), see e.g. (22). The archetype of a 3NF is due to Fujita and Miyazawa (FM) (23), who extended Yukawa's meson exchange idea by sandwiching the pion-nucleon scattering amplitude between nucleon lines, thus generating the 3NF of longest range. In fact, the work of Fujita and Miyazawa has been the seed for many meson-theoretical approaches to the three-nucleon force like the families of Tucson-Melbourne (24; 25), Brazilian (26) or Urbana-Illinois (27; 28) 3NFs.

While the conventional approach as briefly outlined here as enjoyed many successes and is frequently used in e.g. nuclear structure and reaction calculations, it remains incomplete as there are certain deficiencies that can only be overcome based on EFT approaches. These are: (i) it is very difficult - if not impossible - to assign a trustworthy theoretical error, (ii) gauge and chiral symmetries are difficult to implement, (iii) none of the three-nucleon forces is consistent with the underlying nucleon-nucleon interaction models/approaches and (iv) the connection to QCD is not at all obvious. Still, as we will show later, there is a very natural connection between these models and the forces derived from EFT by mapping the complicated physics of the short-distance part of any interaction at length scales $\sim 1/M_\rho$ to the tower of multi-fermion contact interactions that naturally arise in the EFT description (see Sec. II.B).

D. Brief introduction to effective field theory

Effective field theory (EFT) is a general approach to calculate the low-energy behavior of physical systems by exploiting a separation of scales in the system (for reviews see e.g. (29–31)). Its roots can be traced to the renormalization group (32) and the intuitive understanding of ultraviolet divergences in quantum field theory (33). A succinct formulation of the underlying principle was given by Weinberg (34): If one starts from the most general Lagrangian consistent with all symmetries of the underlying interaction, one will get the most general S-matrix consistent with these symmetries. Together with a power counting scheme that specifies which terms are required at a desired accuracy leads to a predictive paradigm for a low-energy theory. The expansion is typically in powers of a low-momentum scale M_{low} which can be the typical external momentum over a high-momentum scale M_{high}. However, what physical scales M_{high} and M_{low} are identified with depends on the considered system. In its most simple setting, consider a theory that is made of two particle species, the light and the heavy ones with $M_{low} \ll M_{high}$. Consider now soft processes in which the energies and momenta are of the order of the light particle mass (the so-called soft scale). Under such conditions, the short-distance physics related to the heavy particles can never be resolved. However, it can be represented by light-particle contact interactions with increasing dimension (number of derivatives). Consider e.g. heavy particle exchange between light ones in the limit that $M_{high} \to \infty$ while keeping the ratio g/M_{high} fixed, with g the light-heavy coupling constant. As depicted in Fig. 3, one can represent such exchange diagrams by a sum of local operators of the light fields with increasing number of derivatives. In a highly symbolic notation

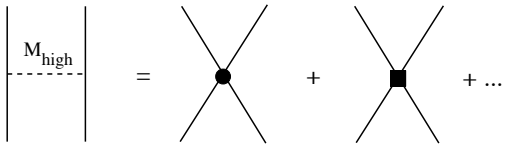

FIG. 3 Expansion of a heavy-particle exchange diagram in terms of local light-particle operators. The solid and dashed lines denote light and heavy particles, respectively. The filled circle and square denote insertions with zero and two derivatives, in order. The ellipses stands for operators with more derivatives.

$$\frac{g^2}{M_{high}^2 - t} = \frac{g^2}{M_{high}^2} + \frac{g^2\, t}{M_{high}^4} + \dots \,, \tag{1.11}$$

with t the squared invariant momentum transfer. In many cases, the corresponding high-energy theory is not known. Still, the framework of EFT offers a predictive and systematic framework for performing calculations in the light particle sector. Denote by $\mathcal{Q}$ a typical energy or momentum of the order of M_{low} and by Λ the hard scale where the EFT will break down. In many cases, this scale is set by the masses of the heavy particles not considered explicitely. In such a setting, any matrix element or Greens function admits an expansion in the small parameter $\mathcal{Q}/\Lambda$ (34)

$$\mathcal{M} = \sum_\nu \left(\frac{\mathcal{Q}}{\Lambda}\right)^\nu \mathcal{F}\left(\frac{\mathcal{Q}}{\mu}, g_i\right) \tag{1.12}$$

where $\mathcal{F}$ is a function of order one (naturalness), μ a regularization scale (related to the UV divergences appearing in the loop graphs) and the g_i denotes a collection

of coupling constants, often called low-energy constants (LECs). These parameterize (encode) the unknown high-energy (short-distance) physics and must be determined by a fit to data (or can be directly calculated if the corresponding high-energy theory is known/can be solved). The counting index ν in general depends on the fields in the effective theory, the number of derivatives and the number of loops. This defines the so-called power counting which allows to categorize all contributions to any matrix element at a given order. It is important to stress that ν must be bounded from below to define a sensible EFT. In QCD e.g. this is a consequence of the spontaneous breaking of its chiral symmetry. The contributions with the lowest possible value of ν define the so-called leading order (LO) contribution, the first corrections with the second smallest allowed value of ν the next-to-leading order (NLO) terms and so on. In contrast to more conventional perturbation theory, the small parameter is not a coupling constant (like, e.g., in Quantum Electrodynamcis) but rather one expands in small energies or momentum, where small refers to the hard scale Λ. The archetype of such a perturbative EFT is chiral perturbation theory that exploits the strictures of the spontaneous and explicit chiral symmetry breaking in QCD (35; 36). Here, the light degrees of freedom are the pions, that are generated through the symmetry violation. Heavier particles like e.g. vector mesons only appear indirectly as they generate local four-pion interactions with four, six, ... derivatives. For a recent review, see Ref. (37). Of course, the pions also couple to heavy matter fields like e.g. nucleons, that can also be included in CHPT, as reviewed by Bernard (38).

So far, we have made the implicit assumption of naturalness, which implies e.g. that the scattering length a is of natural size as e.g. in CHPT, where the scale is set by $1/\Lambda_\chi \simeq 1\,\mathrm{GeV}^{-1} \simeq 0.2\,\mathrm{fm}$. This also implies that there are no bound states close to the scattering thresholds. In many physical systems and of particular interest here, especially in the two-nucleon system, this is not the case, but one rather has to deal with unnaturally large scattering lengths (and also shallow bound states). To be specific, let us consider nucleon-nucleon scattering at very low energies in the $^1S_0$ channel, cf. Eq. (1.10). For such low energies, even the pions can be considered heavy and are thus integrated out. To construct an EFT that is applicable for momenta $p > 1/a$, one must retain all terms $ap \sim 1$ in the scattering matrix. This requires a non-perturbative resummation and is most elegantly done in the power divergence scheme of Kaplan, Savage and Wise (39; 40). This amounts to summing the leading four-nucleon contact term $\sim C_0(\psi^\dagger\psi)^2$ to all orders in C_0 and matching the scale-dependent LEC C_0 to the scattering length. This leads to the T-matrix

$$T = \frac{4\pi}{m}\frac{1}{1/a + ip}\left[1 + \mathcal{O}(p^2)\right] \ , \qquad (1.13)$$

where the expansion around the large scattering length is made explicit. All other effects, like e.g. effective range corrections, are treated perturbatively. This compact and elegant scheme is, however, not sufficient for discussing nuclear processes with momenta $p \geq M_\pi$. We will come back to this topic when we give the explicit construction of the chiral nuclear EFT in sec. II.B. It is important to stress that such EFTs with unnaturally large scattering length can exhibit universal phenomena that can be observed in physical systems which differ in their typical energy scale by many orders of magnitude, for a review see Braaten and Hammer (41). We also remark that there are many subtleties in constructing a proper EFT, but space forbids to discuss these here. Whenever appropriate and/or neccessary, we will mention these in the following sections and provide explicit references.

E. First results from lattice QCD

Lattice QCD (LQCD) is a promising tool to calculate hadron properties ab initio from the QCD Lagrangian on a discretized Euclidean space-time. This requires state-of-the-art high performance computers and refined algorithms to analyse the QCD partition function by Monte Carlo methods. Only recently soft- and hardware developments have become available that allow for full QCD simulations at small enough quark masses (corresponding to pion masses below 300 MeV), large enough volumes (corresponding to spatial dimensions larger than 2.5 fm) and sufficiently fine lattice spacing ($a \simeq 0.05\,\mathrm{fm}$) so that the results are not heavily polluted by computational artefacts and can really be connected to the physical quark masses by sensible chiral extrapolations.

For the nuclear force problem, there are two main developments in LQCD to be reviewed here. These concern the extraction of hadron-hadron scattering lengths from unquenched simulations and the first attempts to construct a nuclear potential. These are groundbreaking studies, but clearly at present one has not yet achieved an accuracy to obtain high-precision predictions for nuclear properties. We look very much forward to the development of these approaches in the years to come.

The first exploratory study of the nucleon-nucleon scattering lengths goes back to Fukugita et al. (42; 43) in the quenched approximation. They make use of an elegant formuala, frequently called the "Lüscher formula", that relates the S-wave scattering length a_0 between two hadrons h_1 and h_2 to the energy shift $\delta E = E_{h_1h_2} - (m_1 + m_2)$ of the two-hadron state at zero relative momentum confined in spatial box of size L^3. It is given by (44–46)

$$\delta E = -\frac{2\pi a_0}{\mu L^3}\left[1 + c_1\frac{a_0}{L} + c_2\frac{a_0^2}{L^2}\right] + \mathcal{O}(L^{-6}) \ , \qquad (1.14)$$

with $\mu = m_1m_2/(m_1 + m_2)$ the reduced mass and $c_1 = 2.837297$ and $c_2 = 6.375183$. A generalization of this formalism was given by Beane et al.(47) utilizing methods developed for the so-called pionless nuclear EFT (EFT

with contact interactions, for a review see e.g. (48)). It reads

$$p\,\cot\delta_0(p) \;=\; \frac{1}{\pi L}\mathcal{S}\left((Lp/2\pi)^2\right)\;,$$
$$\mathcal{S}(\eta) \;=\; \sum_{\vec{j}}^{\Lambda_j}\frac{1}{|\vec{j}\,|^2-\eta} - 4\pi\Lambda_j\;, \qquad (1.15)$$

which gives the location of all energy eigenstates in the box. Here, δ_0 is the S-wave phase shift. The sum over all three-vectors of integers $\vec{j}$ is such that $|\vec{j}\,| < \Lambda_j$ and the limit $\Lambda_j \to \infty$ is implicit. In the limit $L \gg |a_0|$, Eq. (1.15) reduces to the Lüscher formula, Eq. (1.14). On the other hand, for large scattering length, $|(p\cot\delta_0)^{-1}| \gg L$, the energy of the lowest state is given by

$$E_0 = \frac{4\pi^2}{\mu L^2}\left[d_1 + d_2 Lp\cot\delta_0 + \ldots\right]\;, \qquad (1.16)$$

with $d_1 = 0.472895$, $d_2 = 0.0790234$ and $p\cot\delta_0$ is evaluated at the energy $E = 4\pi^2 d_1/(\mu L^2)$. Within this framework, in Ref. (49) the first fully dynamical simulation of the neutron-proton scattering lengths was performed, with a lowest pion mass of 354 MeV. This mass is still too high to perform a precise chiral extrapolation to the physical pion mass, but this calculation clearly demonstrates the feasilbilty of this approach (see also sec. II.H). This scheme can also be extended to hyperon-nucleon interactions, see (50). A first signal for $\pi\Lambda$ and $n\Sigma^-$ scattering was reported in Ref. (51). For a recent review on these activities of the NPLQCD collaboration, we refer the reader to (52).

Another interesting development was initiated and carried out by Aoki, Hatsuda and Ishii (53). They have generalized the two-center Bethe-Salpeter wavefunction approach of the CP-PACS collaboration (54), which offers an alternative to Lüscher's formula, to the two-nucleon (NN) system. Given an interpolating field for the neutron and for the proton, the NN potential can be defined from the properly reduced 6-quark Bethe-Salpeter amplitude $\phi(\vec{r})$. The resulting Lippmann-Schwinger equation defines a non-local potential for a given, fixed separation $r = |\vec{r}|$. Performing a derivative expansion, the central potential $V_c(r)$ at a given energy E is extracted from

$$V_C(r) = E + \frac{1}{m}\frac{\vec{\nabla}^2\phi(r)}{\phi(r)}\;. \qquad (1.17)$$

Monte Carlo Simulations are then performed to generate the 6-quark Bethe-Salpeter amplitude in a given spin and isospin state of the two-nucleon system on a large lattice, $V = (4.4\,\mathrm{fm})^4$ in the quenched approximation for pion masses between 380 and 730 MeV. Despite these approximations, the resulting effective potential extracted using Eq. (1.17) shares the features of the phenomenological NN potentials - a hard core (repulsion) at small separation surrounded by an attractive well at intermediate and larger distances, see Fig. 4. Furthermore, the

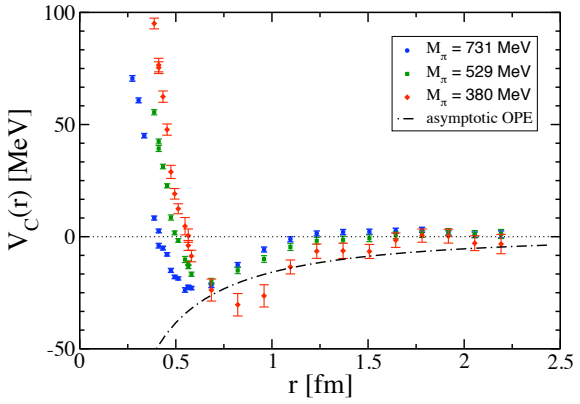

FIG. 4 Effective potential in the $^1S_0$ channel for three different quark masses in quenched LQCD after Ref. (55). The dashed line is the asymptotic OPEP for $M_\pi = 380\,\mathrm{MeV}$, $m = 1.2\,\mathrm{GeV}$ and $g_{iN}^2/(4\pi) = 14.0$. We are grateful to Dr. N. Ishii for providing us with the data.

asymptotic form of this potential has exactly the form of the OPE, provided one rescales the formula

$$V_C^{\mathrm{OPE}}(r) = \frac{g_{\pi N}^2}{4\pi}\,\boldsymbol{\tau}_1\cdot\boldsymbol{\tau}_2\frac{\vec{\sigma}_1\cdot\vec{\sigma}_2}{3}\left(\frac{M_\pi}{2m}\right)^2\frac{\mathrm{e}^{-M_\pi r}}{r} \qquad (1.18)$$

with the pion and nucleon masses used in the simulations but keeping the pion-nucleon coupling at its physical value, $g_{\pi N}^2/(4\pi) \simeq 14.0$. These interesting results have led to some enthusiastic appraisal, see e.g. (56). However, it is important to stress that the so-calculated potential is not unique, especially its properties at short distances, since it depends on the definition of the interpolating nucleon fields. Furthermore, the quenched approximation is known to have uncontrolled systematic uncertainties as it does not even define a quantum field theory. In this context, the authors of Ref. (54) report on the numerical absence of the large-distance-dominating η-exchange from the flavor-singlet hair-pin diagram. Still, one would like to see this promising calculation repeated with dynamical quarks of sufficiently small masses. In Ref. (57) this framework was used to study the ΞN interaction. Interestingly, the central potential of the $p\Xi^0$ interaction looks very similar to the central np potential. It would be interesting to extend these calculations to other hyperon-nucleon channels and also study the effects of SU(3) symmetry breaking. We will come back to these issues in the context of an three-flavor chiral EFT in sec. II.F. For recent developments in this scheme concerning the calculation of the tensor force, the energy dependence of the NN potential and preliminary results for full QCD (2+1 flavors), see the talks by Aoki, Ishii, and Nemura at the Lattice 2008 conference (58).

F. Observables and not-so observable quantities

There is an extensive literature, primarily from the sixties and seventies, on the role of off-shell physics in nuclear phenomena (see, e.g., Ref. (59) and references therein). This includes not only few-body systems (e.g., the triton) and nuclear matter, but interactions of two-body systems with external probes, such as nucleon-nucleon bremstrahlung and the electromagnetic form factors of the deuteron. The implicit premise was that there is a true underlying potential governing the nucleon-nucleon force, so that its off-shell properties can be determined. Indeed, the nuclear many-body problem has traditionally been posed as finding approximate solutions to the many-particle Schrödinger equation, given a fundamental two-body interaction that reproduces two-nucleon observables.

In contrast, effective field theories *are* determined completely by on-energy-shell information, up to a well-defined truncation error. In writing down the most general Lagrangian consistent with the symmetries of the underlying theory, many-body forces arise naturally. Even though they are usually suppressed at low energies, they enter at some order in the EFT expansion. These many-body forces have to be determined from many-body data. The key point is, however, that no off-energy-shell information is needed or experimentally accessible. A fundamental theorem of quantum field theory states that physical observables (or more precisely, S-matrix elements) are independent of the choice of interpolating fields that appear in a Lagrangian (60; 61). Equivalently, observables are invariant under a change of field variables in a field theory Lagrangian (or Hamiltonian):

$$\psi(x) \to \psi(x) + \eta P[\psi]\,, \tag{1.19}$$

where $P[\psi]$ is a local polynomial of the field ψ and its derivatives and η is an arbitray counting parameter. Newly generated contributions to observables have to cancel separately at each order in η. This "equivalence theorem" holds for renormalized field theories. In an EFT, one exploits the invariance under field redefinitions to eliminate redundant terms in the effective Lagrangian and to choose the most convenient or efficient form for practical calculations (62–66). Since off-shell Green's functions and the corresponding off-shell amplitudes *do* change under field redefinitions, one must conclude that off-shell properties are unobservable.

Several recent works have emphasized from a field theory point of view the impossibility of observing off-shell effects. In Refs. (67; 68), model calculations were used to illustrate how apparent determinations of the two-nucleon off-shell T-matrix in nucleon-nucleon bremstrahlung are illusory, since field redefinitions shift contributions between off-shell contributions and contact interactions. Similarly, it was shown in Ref. (69) that Compton scattering on a pion cannot be used to extract information on the off-shell behavior of the pion form factor. The authors of Refs. (70; 71) emphasized the nonuniqueness of chiral Lagrangians for three-nucleon forces and pion production. Field redefinitions lead to different off-shell forms that yield the same observables within a consistent power counting. In Ref. (72), an interaction proportional to the equation of motion is shown to have no observable consequence for the deuteron electromagnetic form factor, even though it contributes to the off-shell T-matrix.

In systems with more than two nucleons, one can trade off-shell, two-body interactions for many-body forces. This explains how two-body interactions related by unitary transformations can predict different binding energies for the triton (73) if many-body forces are not consistently included. These issues were discussed from the viewpoint of unitary transformations in Refs. (74) and (75). The extension to many-fermion systems in the thermodynamic limit was considered in (76). The effects of field redefinitions were illustrated using the EFT for the dilute Fermi gas (77). If many-body interactions generated by the field redefinitions are neglected, a Coester line similar to the one observed for nuclear matter (78) is generated. Moreover, the connection to more traditional treatments using unitary transformations was elucidated. The question of whether occupation numbers and momentum distributions of nucleons in nuclei are observables was investigated in Ref. (79). Field redefinitions lead to variations in the occupation numbers and momentum distributions that imply the answer is negative. The natural size of the inherent ambiguity (or scheme dependence) in these quantities is determined by the applicability of the impulse approximation. Only if the impulse approximation is well justified, the ambiguity is small and these quantities are approximately scheme independent. This has important implications for the interpretation of $(e,e'p)$ experiments with nuclei. Whether the stark difference in occupation numbers between non-relativistic and relativistic Brueckner calculations can be explained by this ambiguity is another interesting question (80).

II. EFT FOR FEW-NUCLEON SYSTEMS: FOUNDATIONS AND APPLICATIONS

A. EFT with contact interactions and universal aspects

In nuclear physics, there are a number of EFTs which are all useful for a certain range of systems (cf. Fig. 2). The simplest theories include only short range interactions and even integrate out the pions. At extremely low energies, M_{high} is given by the NN scattering lengths and one can formulate a perturbative EFT in powers of of the typical momentum k divided by M_{high}. Since the NN scattering lengths are large this theory has a very limited range of applicability. It is therefore useful to construct another EFT with short-range interactions that resums the interactions generating the large scattering length. This so-called pionless EFT can be understood as an ex-

pansion around the limit of infinite scattering length or equivalently around threshold bound states. Its breakdown scale is set by one-pion exchange, $M_{high} \sim M_\pi$, while $M_{low} \sim 1/a \sim k$. For momenta k of the order of the pion mass M_π, pion exchange becomes a long-range interaction and has to be treated explicitly. This leads to the chiral EFT whose breakdown scale M_{high} is set by the chiral symmetry breaking scale Λ_χ and will be discussed in detail below.

The pionless theory relies only on the large scattering length and is independent of the mechanism responsible for it. It is very general and can be applied in systems ranging from ultracold atoms to nuclear and particle physics. It is therefore ideally suited to unravel universal phenomena driven by the large scattering length such as limit cycle physics (81; 82) and the Efimov effect (83). For recent reviews of applications to the physics of ultracold atoms, see Refs. (41; 84). Here we consider applications of this theory in nuclear physics.

The pionless EFT is designed to reproduce the well known effective range expansion. The leading order Lagrangian can be written as:

$$\begin{aligned}\mathcal{L} &= N^\dagger \left(i\partial_0 + \frac{\vec{\nabla}^2}{2m} \right) N \\ &- C_0^t \left(N^T \tau_2 \sigma_i \sigma_2 N\right)^\dagger \left(N^T \tau_2 \sigma_i \sigma_2 N\right) \\ &- C_0^s \left(N^T \sigma_2 \tau_a \tau_2 N\right)^\dagger \left(N^T \sigma_2 \tau_a \tau_2 N\right) + \ldots , \quad (2.1)\end{aligned}$$

where the dots represent higher-order terms suppressed by derivatives and more nucleon fields. The Pauli matrices σ_i (τ_a) operate in spin (isospin) space, respectively. The contact terms proportional to C_0^t (C_0^s) correspond to two-nucleon interactions in the ^{3}S$_1$ (^{1}S$_0$) NN channels. Their renormalized values are related to the corresponding large scattering lengths a_t and a_s in the spin-triplet and spin-singlet channels, respectively. The exact relation, of course, depends on the renormalization scheme. Various schemes can be used, such as a momentum cutoff or dimensional regularization. Convenient schemes that have a manifest power counting at the level of individual diagrams are dimensional regularization with PDS subtraction, where poles in 2 and 3 spatial dimensions are subtracted (40), or momentum subtractions schemes as in (85). However, a simple momentum cutoff can be used as well.

Since the scattering lengths are set by the low-momentum scale $a \sim 1/M_{low}$, the leading contact interactions have to be resummed to all orders (40; 86). The nucleon-nucleon scattering amplitude in the ^{3}S$_1$ (^{1}S$_0$) channels is obtained by summing the so-called bubble diagrams with the C_0^t (C_0^s) interactions shown in Fig. 5. This summation gives the exact solution of the Lippmann-Schwinger equation for the C_0^t or C_0^s interactions. Higher order derivative terms which are not shown explicitly in Eq. (2.1) reproduce higher order terms in the effective range expansion. Since these terms are natural and their size is set by M_{high}, their contribution at

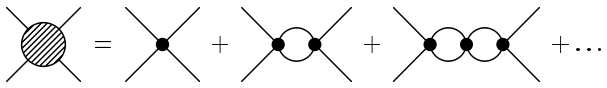

FIG. 5 The bubble diagrams with the contact interaction C_0^t or C_0^s contributing to the two-nucleon scattering amplitude.

low energies is suppressed by powers of M_{low}/M_{high} and can be treated in perturbation theory. The subleading correction is given by the effective range $r_0 \sim 1/M_{high}$ and the corresponding diagrams are illustrated in Fig. 6. The renormalized S-wave scattering amplitude to next-to-leading order in a given channel then takes the form

$$T_2(k) = \frac{4\pi}{m} \frac{1}{-1/a - ik} \left[1 - \frac{r_0 k^2/2}{-1/a - ik} + \ldots \right] \quad (2.2)$$

where k is the relative momentum of the nucleons and the dots indicate corrections of order $(M_{low}/M_{high})^2$ for typical momenta $k \sim M_{low}$. The pionless EFT becomes very useful in the two-nucleon sector when external currents are considered and has been applied to a variety of electroweak processes. These calculations are reviewed in detail in Refs. (48; 87). More recently Christlmeier and Grießhammer have calculated low-energy deuteron electrodisintegration in the framework of the pionless EFT (88). For the double differential cross sections of the $d(e,e')$ reaction at $\theta = 180^\circ$ excellent agreement was found with a recent experiment at S-DALINAC (89).[#1] The double-differential cross section for an incident electron energy $E_0 = 27.8$ MeV and $\theta = 180^\circ$ is shown in Fig. 7. The data were used to precisely map the $M1$ response which governs the reaction $np \to d\gamma$ relevant to big-bang nucleosythesis. Finally, the reaction $pp \to pp\pi^0$ near threshold was studied by Ando (90).

We now proceed to the three-nucleon system. Here it is convenient (but not mandatory) to rewrite the theory using so-called "dimeron" auxilliary fields (91). We need two dimeron fields, one for each S-wave channel: (i) a field t_i with spin (isospin) 1 (0) representing two nucleons interacting in the $^3S_1$ channel (the deuteron) and (ii) a field s_a with spin (isospin) 0 (1) representing two nucleons

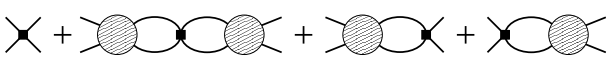

FIG. 6 Diagrams for the inclusion of higher order contact interactions.

[#1] However, there is a disagreement between theory and data for the small longitudinal-transverse interference contribution σ_{LT} that is currently not understood (88).

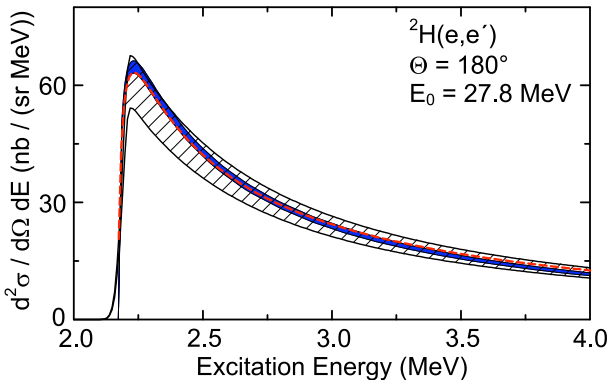

FIG. 7 Double-differential cross sections of the $^2\mathrm{H}(e,e')$ reaction with errors (hatched bands) extracted from the experiment. The gray bands and dashed lines are calculations in pionless EFT and a potential model. Figure courtesy of H.W. Grießhammer.

interacting in the $^1S_0$ channel (92):

$$\begin{aligned}\mathcal{L} &= N^\dagger\Big(i\partial_t + \frac{\vec\nabla^2}{2m}\Big)N - t_i^\dagger\Big(i\partial_t - \frac{\vec\nabla^2}{4m} - \Delta_t\Big)t_i \\ &- s_a^\dagger\Big(i\partial_t - \frac{\vec\nabla^2}{4m} - \Delta_s\Big)s_a - \frac{g_t}{2}\Big(t_i^\dagger N^T\tau_2\sigma_i\sigma_2 N + h.c.\Big) \\ &- \frac{g_s}{2}\Big(s_a^\dagger N^T\sigma_2\tau_a\tau_2 N + h.c.\Big) - G_3 N^\dagger\Big[g_t^2(t_i\sigma_i)^\dagger(t_j\sigma_j) \\ &+ \frac{g_t g_s}{3}\left((t_i\sigma_i)^\dagger(s_a\tau_a) + h.c.\right) + g_s^2(s_a\tau_a)^\dagger(s_b\tau_b)\Big]N \\ &+ \ldots\,, \end{aligned} \tag{2.3}$$

where i,j are spin and a,b are isospin indices while g_t, g_s, Δ_t, Δ_s and G_3 are the bare coupling constants. This Lagrangian goes beyond leading order and already includes the effective range terms. The coupling constants g_t, Δ_t, g_s, Δ_s are matched to the scattering lengths a_α and effective ranges $r_{0\alpha}$ in the two channels ($\alpha = s,t$). Alternatively, one can match to the position of the bound state/virtual state pole γ_α in the T-matrix instead of the scattering length which often improves convergence (93). The two quantities are related through:

$$\gamma_\alpha = \frac{1}{r_{0\alpha}}\left(1 - \sqrt{1 - 2r_{0\alpha}/a_\alpha}\right)\,, \tag{2.4}$$

where $\alpha = s,t$. The term proportional to G_3 constitutes a Wigner-$SU(4)$ symmetric three-body interaction. It only contributes in the spin-doublet S-wave channel. When the auxilliary dimeron fields t_i and s_a are integrated out, an equivalent form containing only nucleon fields is obtained. At leading order when the effective range corrections are neglected, the spatial and time derivatives acting on the dimeron fields are omitted and the field is static. The coupling constants g_α and Δ_α, $\alpha = s,t$ are then not independent and only the combination g_α^2/Δ_α enters in observables. This combination can then be matched to the scattering length or pole position.

The simplest three-body process to consider is neutron-deuteron scattering below the breakup threshold. In order to focus on the main aspects of renormalization, we suppress all spin-isospin indices and complications from coupled channels in the three-nucleon problem. This corresponds to a system of three spinless bosons with large scattering length. If the scattering length is positive, the bosons form a two-body bound state analog to the deuteron which we call dimeron. The leading order integral equation for boson-dimeron scattering is shown schematically in Fig. 8. For total orbital angular momentum $L = 0$, it takes the following form:

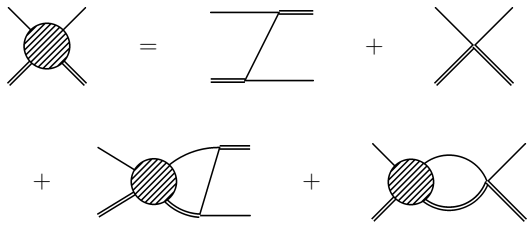

FIG. 8 The integral equation for the boson-dimeron scattering amplitude. The single (double) line indicates the boson (dimeron) propagator.

$$\begin{aligned}T_3(k,p;\,E) &= \frac{16}{3a}M(k,p;\,E) + \frac{4}{\pi}\int_0^\Lambda dq\,q^2\,T_3(k,q;\,E) \\ &\times\frac{M(q,p;\,E)}{-1/a + \sqrt{3q^2/4 - mE - i\epsilon}}\,,\end{aligned} \tag{2.5}$$

where the inhomogeneous term reads

$$M(k,p;\,E) = \frac{1}{2kp}\ln\left(\frac{k^2+kp+p^2-mE}{k^2-kp+p^2-mE}\right) + \frac{H(\Lambda)}{\Lambda^2}\,. \tag{2.6}$$

Here, H determines the strength of the three-body force $G_3(\Lambda) = 2mH(\Lambda)/\Lambda^2$ which enters already at leading order and Λ is a UV cutoff introduced to regularize the integral equation. The magnitude of the incoming (outgoing) relative momenta is k (p) and $E = 3k^2/(4m) - 1/(ma^2)$. The on-shell point corresponds to $k = p$ and the phase shift can be obtained via $k\cot\delta = 1/T_3(k,k;\,E) + ik$. For $H = 0$ and $\Lambda\to\infty$, Eq. (2.5) reduces to the STM equation first derived by Skorniakov and Ter-Martirosian (94). It is well known that the STM equation has no unique solution (95). The regularized equation has a unique solution for any given (finite) value of the ultraviolet cutoff Λ but the amplitude in the absence of the three-body force shows an oscillatory behavior on $\ln\Lambda$. Cutoff independence of the amplitude is restored by an appropriate "running" of $H(\Lambda)$ which turns out to be a limit cycle (96; 97):

$$H(\Lambda) = \frac{\cos[s_0\ln(\Lambda/\Lambda_*) + \arctan s_0]}{\cos[s_0\ln(\Lambda/\Lambda_*) - \arctan s_0]}\,, \tag{2.7}$$

where Λ_* is a dimensionful three-body parameter generated by dimensional transmutation. Adjusting Λ_* to a single three-body observable allows to determine all other

low-energy properties of the three-body system. Note that the choice of the three-body parameter Λ_* is not unique and there are other definitions more directly related to experiment (41). Because $H(\Lambda)$ in Eq. (2.7) vanishes for certain values of the cutoff Λ it is possible to eliminate the explicit three-body force from the equations by working with a fixed cutoff that encodes the dependence on Λ_*. This justifies tuning the cutoff Λ in the STM equation to reproduce a three-body datum and using the same cutoff to calculate other observables as suggested by Kharchenko (98). Equivalently, a subtraction can be performed in the integral equation (99; 100). In any case, one three-body input parameter is needed for the calculation of observables. A comprehensive study of the range corrections to the three-boson spectrum was carried out in Ref. (101). The authors showed that all range corrections vanish in the unitary limit due to the discrete scale invariance. While the corrections proportional to r_0/a vanish trivially, this includes also the corrections proportional to $\kappa_* r_0$ where $\kappa_* = \sqrt{mB_3^*}$ is the binding momentum of the Efimov state fixed by the chosen renormalization condition. Moreover, they have calculated the corrections to the Efimov spectrum for finite scattering length. The range corrections are negligible for the shallow states but become important for the deeper bound states.

The integral equations for the three-nucleon problem derived from the Lagrangian (2.3) are a generalization of Eq. (2.5). (For their explicit form and derivation, see e.g. Ref. (102).) For S-wave nucleon-deuteron scattering in the spin-quartet channel only the spin-1 dimeron field contributes. This integral equation has a unique solution for $\Lambda \to \infty$ and there is no three-body force in the first few orders. The spin-quartet scattering phases can therefore be predicted to high precision from two-body data (103; 104). In the spin-doublet channel both dimeron fields as well as the the three-body force in the Lagrangian (2.3) contribute (92). This leads to a pair of coupled integral equations for the T-matrix. Thus, one needs a new parameter which is not determined in the 2N system in order to fix the (leading) low-energy behavior of the 3N system in this channel. The three-body parameter gives a natural explanation of universal correlations between different three-body observables such as the Phillips line, a correlation between the triton binding energy and the spin-doublet neutron-deuteron scattering length (105). These correlations are purely driven by the large scattering length independent of the mechanism responsible for it. As a consequence, they occur in atomic systems such as ^{4}He atoms as well (41).

Higher-order corrections to the amplitude including the ones due to 2N effective range terms can be included perturbatively. This was first done at NLO for the scattering length and triton binding energy in (106) and for the energy dependence of the phase shifts in (99). In Refs. (102; 107), it was demonstrated that it is convenient to iterate certain higher order range terms in order to extend the calculation to N^{2}LO. Here, also a subleading three-body force was included as required by dimensional analysis. More recently, Platter and Phillips showed using the subtractive renormalization that the leading three-body force is sufficient to achieve cutoff independence up to N^{2}LO in the expansion in M_{low}/M_{high} (108). The results for the spin-doublet neutron-deuteron scattering phase shift at LO (92), NLO (99), and N^{2}LO (109) are shown in Fig. 9. There is excellent agreement with the available phase shift analysis and a calculation using a phenomenological NN interaction. Whether there is a suppression of the subleading three-body force or simply a correlation between the leading and subleading contributions is not fully understood. The extension to 3N channels with higher orbital angular momentum is straightforward (110) and three-body forces do not appear until very high orders. A general counting scheme for three-body forces based on the asymptotic behavior of the solutions of the leading order STM equation was proposed in (111). A complementary approach to the few-nucleon problem is given by the renormalization group where the power counting is determined from the scaling of operators under the renormalization group transformation (32). This method leads to consistent results for the power counting (112–114). Universal low-energy properties of few-body systems with short-range interactions and large two-body scattering length were reviewed in (41). (See also (115) for an early work on this subject.) Three-body calculations with external currents are still in their infancy. However, a few exploratory calculations have been carried out. Universal properties of the triton charge form factor were investigated in Ref. (116) and neutron-deuteron radiative capture was calculated in Refs. (117; 118). This opens the possibility to carry out accurate calculations of electroweak reactions at very low energies for astrophysical processes.

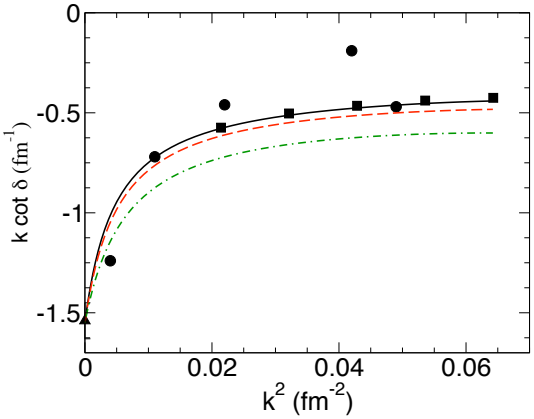

FIG. 9 Phase shifts for neutron-deuteron scattering below the deuteron breakup at LO (dash-dotted line), NLO (dashed line), and N^{2}LO (solid line). The filled squares and circles give the results of a phase shift analysis and a calculation using AV18 and the Urbana IX three-body force, respectively. Figure courtesy of L. Platter.

The pionless approach has also been extended to the

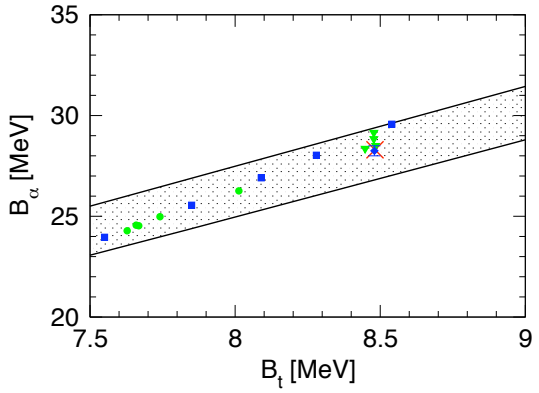

FIG. 10 The Tjon line correlation as predicted by the pionless theory. The grey circles and triangles show various calculations using phenomenological potentials (121). The squares show the results of chiral EFT at NLO for different cutoffs while the diamond gives the N^{2}LO result (122; 123). The cross shows the experimental point.

four-body sector (119; 120). In order to be able to apply the Yakubovsky equations, an equivalent effective quantum mechanics formulation was used. The study of the cutoff dependence of the four-body binding energies revealed that no four-body parameter is required for renormalization at leading order. As a consequence, there are universal correlations in the four-body sector which are also driven by the large scattering length. The best known example is the Tjon line: a correlation between the triton and alpha particle binding energies, B_t and B_α, respectively. Of course, higher order corrections break the exact correlation and generate a band. In Fig. 10, we show this band together with some some calculations using phenomenological potentials (121) and a chiral EFT potential with explicit pions (122; 123). All calculations with interactions that give a large scattering length must lie within the band. Different short-distance physics and/or cutoff dependence should only move the results along the band. This can for example be observed in the NLO results with the chiral potential indicated by the squares in Fig. 10 or in the few-body calculations with the low-momentum NN potential $V_{\rm low\,k}$ carried out in Ref. (124). The $V_{\rm low\,k}$ potential is obtained from phenomenological NN interactions by intergrating out high-momentum modes above a cutoff Λ but leaving two-body observables (such as the large scattering lengths) unchanged. The results of few-body calculations with $V_{\rm low\,k}$ are not independent of Λ but lie all close to the Tjon line (cf. Fig. 2 in Ref. (124)). The studies of the four-body system in the pionless theory were extendend further in Ref. (125). Here the dependence of the four-body bound state spectrum on the two-body scattering length was investigated in detail and summarized in a generalized Efimov plot for the four-body spectrum.

The question of whether a four-body parameter has to enter at leading order was reanalyzed by Yamashita et al. (126). Within the renormalized zero-range model, they found a strong sensitivity of the deepest four-body energy to a four-body subtraction constant in their equations. They motivated this observation from a general model-space reduction of a realistic two-body interaction close to a Feshbach resonance. The results of Ref. (119) for the ^{4}He tetramer that include a four-body parameter were also reproduced. Yamashita et al. concluded that a four-body parameter should generally enter at leading order. They argued that four-body systems of ^{4}He atoms and nucleons (where this sensitivity is absent (119; 120; 124)) are special because repulsive interactions strongly reduce the probability to have four particles close together. However, the renormalization of the four-body problem was not explicitly verified in their calculation. Another drawback of their analysis is the focus on the deepest four-body state only. Therefore, their findings could be an artefact of their particular regularization scheme. Another recent study by von Stecher and collaborators (127) confirmed the absence of a four-body parameter for shallow states while some sensitivity was found for the deepest four-body state.

The pionless theory has also been extended to more than four particles using it within the no-core shell model approach. Here the expansion in a truncated harmonic oscillator basis is used as the ultraviolet regulator of the EFT. The effective interaction is determined directly in the model space, where an exact diagonalization in a complete many-body basis is performed. In Ref. (128), the 0^+ excited state of ^{4}He and the ^{6}Li ground state were calculated using the deuteron, triton, alpha particle ground states as input. The first $(0^+;0)$ excited state in ^{4}He is calculated within 10% of the experimental value, while the ^{6}Li ground state comes out at about 70% of the experimental value in agreement with the 30 % error expected for the leading order approximation. These results are promising and should be improved if range corrections are included. Finally, the spectrum of trapped three- and four-fermion systems was calculated using the same method (129). In this case the harmonic potential is physical and not simply used as an ultraviolet regulator.

B. Chiral EFT for few nucleons: foundations

The extension of the previously discussed EFT with contact interactions to higher energies requires the inclusion of pions as explicit degrees of freedom. The interaction between pions and nucleons can be described in a systematic way using chiral perturbation theory. In contrast, the interaction between the nucleons is strong and leads to nonperturbative phenomena at low energy such as e.g. shallow-lying bound states. This breakdown of perturbation theory can be linked to the fact that the interaction between the nucleons is *not* suppressed in the chiral limit contrary to the pion and pion-nucleon interactions. Moreover, an additional enhancement occurs for Feynman diagrams involving two and

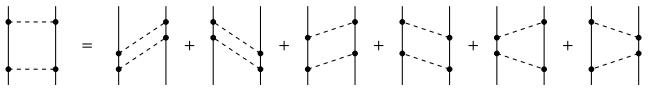

FIG. 11 Representation of the two-pion exchange Feynman diagram in terms of time-ordered graphs. Solid and dashed lines represent nucleons and pions, respectively.

more nucleons due to the appearance of the so-called pinch singularities in the limit of the infinite nucleon mass. Although such infrared singularities disappear if one keeps the nucleon mass at its physical value, they do generate large enhancement factors which destroy the chiral power counting. This can be more easily understood utilizing the language of time-ordered perturbation theory. Consider, for example, the two-pion exchange box diagram shown in Fig. 11. While all intermediate states in the first two time-ordered graphs, often referred to as irreducible, involve at least one virtual pion and thus lead to energy denimonators of the expected size, $E - E_i \sim M_\pi$, the remaining reducible diagrams involve an intermediate state with nucleons only which produces unnaturally small energy denominators of the order $E - E_i \sim M_\pi^2/m \ll M_\pi$. Clearly, the enhanced reducible time-ordered diagrams are nothing but the iterations of the Lippmann-Schwinger equation with the kernel which contains all possible irreducible diagrams and defines the nuclear Hamiltonian. It is free from infrared enhancement factors and can be worked out systematically using the machinery of chiral perturbation theory as suggested in Weinberg's seminal work (130; 131).[#2] This natural reduction to the quantum mechanical A-body problem is a welcome feature for practical calculations as it allows to apply various existing few-body techniques such as e.g. the Faddeev-Yakubovsky scheme, the no-core shell model, Green's function Monte Carlo and hyperspherical harmonics methods. On the other hand, the framework offers a systematic and perturbative scheme to derive nuclear forces and current operators in harmony with the chiral symmetry of QCD. The expansion parameter is given by the ratio Q/Λ where Q is the soft scale associated with the pion mass and/or external nucleon momenta and Λ is the pertinent hard scale. For a given connected irreducible diagram with N nucleons, L pion loops and V_i vertices of type i, the power ν of the soft scale Q which determines its importance can be obtained based on naive dimensional analysis (i.e. assuming classical scaling dimensions for various operators in the effective Lagrangian):

$$\nu = -4+2N+2L+\sum_i V_i\Delta_i\,, \quad \Delta_i = d_i+\frac{1}{2}n_i-2\,. \quad (2.8)$$

Here, n_i is the number of nucleon field operators and d_i the number of derivatives and/or insertions of M_π. The spontaneously broken chiral symmetry of QCD guarantees $\Delta_i \geq 0$. As a consequence, the chiral dimension ν is bounded from below, and only a finite number of diagrams contribute at a given order. In addition, Eq. (2.8) provides a natural explanation to the dominance of the two-nucleon interactions and the hierarchy of nuclear forces observed in nuclear physics. In particular, it implies that two-, three-, and four-nucleon forces start to contribute at orders $\nu = 0$, 2 and 4, respectively. Notice that as argued in Ref. (131), the nucleon mass m should be counted as $Q/m \sim Q^2/\Lambda^2$ (which implies that $m \gg \Lambda$) in order to maintain consistency with the appearance of shallow-lying bound states.[#3] Notice further that according to this counting rule, the momentum scale associated with the real pion production is treated as the hard scale, $\sqrt{mM_\pi} \sim \Lambda$, and needs not be explicitly kept track of, see also (138) and section II.E for a related discussion. Clearly, such a framework is only applicable at energies well below the pion production threshold. We also emphasize that the validity of the naive dimensional scaling rules for few-nucleon contact operators has been questioned in Refs. (139; 140). We will come back to this issue in section II.C.

Before discussing the chiral expansion of the nuclear forces it is important to clarify the relation between the underlying chiral Lagrangian for pions and nucleons and the nuclear Hamiltonian we are finally interested in. The derivation of the nuclear potentials from field theory is an old and extensively studied problem in nuclear physics. Different approaches have been developed in the fifties of the last century in the context of the so-called meson theory of nuclear forces, see e.g. the review article (141). In the modern framework of chiral EFT, the most frequently used methods besides the already mentioned time-ordered perturbation theory are the ones based on S-matrix and the unitary transformation. In the former scheme, the nuclear potential is defined through matching the amplitude to the iterated Lippmann-Schwinger equation (142). In the second approach, the potential is obtained by applying an appropriately choosen unitary transformation to the underlying pion-nucleon Hamiltonian which eliminates the coupling between the purely nucleonic Fock space states and the ones which contain pions, see (143) for more details. We stress that both methods lead to *energy-independent* interactions as opposed by the ones obtained in time-ordered perturbation

[#2] An alternative framework based on the perturbative treatment of the pion exchange contributions has been introduced by Kaplan, Savage and Wise (39; 40), see (48; 87) for review articles. As shown in Refs. (132–134), the perturbative inclusion of pions does not allow to significantly increase the applicability range of the theory as compared to pionless EFT. For yet different proposals to include pions in EFT for the nucleon-nucleon system see Refs. (135–137).

[#3] This statement only applies for the power counting based on naive dimensional analysis.

theory. The energy independence of the potential is a welcome feature which enables applications to three- and more-nucleon systems.

We are now in the position to discuss the structure of the nuclear force at lowest orders of the chiral expansion. The leading-order (LO) contribution results, according to Eq. (2.8), from two-nucleon tree diagrams constructed from the Lagrangian of lowest dimension $\Delta_i = 0$, $\mathcal{L}^{(0)}$, which has the following form in the heavy-baryon formulation (144; 145):

$$\begin{aligned}
\mathcal{L}_{\pi}^{(0)} &= \frac{F^2}{4}\langle \nabla^\mu U \nabla_\mu U^\dagger + \chi_+ \rangle \,, \qquad (2.9)\\
\mathcal{L}_{\pi N}^{(0)} &= \bar{N}\left(i\, v\cdot D + \mathring{g}_A \; u\cdot S \right) N \,,\\
\mathcal{L}_{NN}^{(0)} &= -\frac{1}{2} C_S (\bar{N}N)(\bar{N}N) + 2 C_T (\bar{N} S N)\cdot(\bar{N} S N) \,,
\end{aligned}$$

where N, v_μ and $S_\mu \equiv (1/2) i\gamma_5 \sigma_{\mu\nu} v^\nu$ denote the large component of the nucleon field, the nucleon four-velocity and the covariant spin vector, respectively. The brackets $\langle \ldots \rangle$ denote traces in the flavor space while F and $\mathring{g}_A$ refer to the chiral-limit values of the pion decay and the nucleon axial vector coupling constants. The low-energy constants (LECs) C_S and C_T determine the strength of the leading NN short-range interaction. Further, the unitary 2×2 matrix $U(\boldsymbol{\pi}) = u^2(\boldsymbol{\pi})$ in the flavor space collects the pion fields,

$$U(\boldsymbol{\pi}) = 1 + \frac{i}{F}\boldsymbol{\tau}\cdot\boldsymbol{\pi} - \frac{1}{2F^2}\boldsymbol{\pi}^2 + \mathcal{O}(\pi^3) \,, \qquad (2.10)$$

where τ_i denotes the isospin Pauli matrix. The covariant derivatives of the nucleon and pion fields are defined via $D_\mu = \partial_\mu + [u^\dagger, \partial_\mu u]/2$ and $u_\mu = i(u^\dagger \partial_\mu u - u \partial_\mu u^\dagger)$. The quantity $\chi_+ = u^\dagger \chi u^\dagger + u \chi^\dagger u$ with $\chi = 2B\mathcal{M}$ involves the explicit chiral symmetry breaking due to the finite light quark masses, $\mathcal{M} = \mathrm{diag}(m_u, m_d)$. The constant B is related to the value of the scalar quark condensate in the chiral limit, $\langle 0|\bar{u}u|0\rangle = -F^2 B$, and relates the pion mass M_π to the quark mass m_q via $M_\pi^2 = 2Bm_q + \mathcal{O}(m_q^2)$. For more details on the notation and the complete expressions for the pion-nucleon Lagrangian including up to four derivatives/M_π-insertions the reader is referred to (146). Expanding the effective Lagrangian in Eqs. (2.9) in powers of the pion fields one can easily verify that the only possible connected two-nucleon tree diagrams are the one-pion exchange and the contact one, see the first line in Fig. 12, yielding the following potential in the two-nucleon center-of-mass system (CMS):

$$V_{\rm 2N}^{(0)} = -\frac{g_A^2}{4F_\pi^2}\frac{\vec{\sigma}_1\cdot\vec{q}\,\vec{\sigma}_2\cdot\vec{q}}{\vec{q}^{\,2}+M_\pi^2}\boldsymbol{\tau}_1\cdot\boldsymbol{\tau}_2 + C_S + C_T \vec{\sigma}_1\cdot\vec{\sigma}_2 \,, \quad (2.11)$$

where the superscript of $V_{\rm 2N}$ denotes the chiral order ν, σ_i are the Pauli spin matrices, $\vec{q} = \vec{p}\,' - \vec{p}$ is the nucleon momentum transfer and $\vec{p}$ ($\vec{p}\,'$) refers to initial (final) nucleon momenta in the CMS. Further, $F_\pi = 92.4$ MeV and $g_A = 1.267$ denote the pion decay and the nucleon axial coupling constants, respectively.

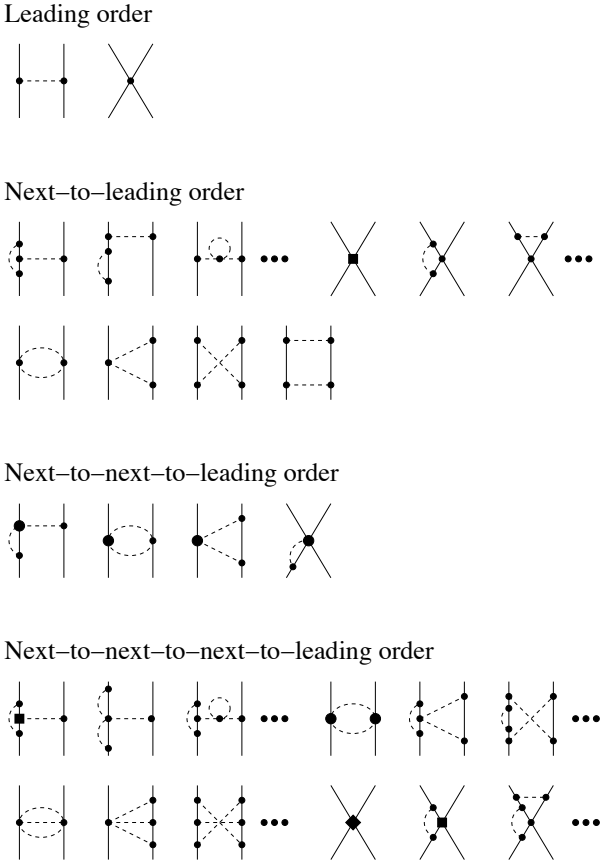

FIG. 12 Chiral expansion of the two-nucleon force up to N^{3}LO. Solid dots, filled circles, squares and diamonds denote vertices with $\Delta_i = 0$, 1, 2 and 4, respectively. Only irreducible contributions of the diagrams are taken in to account as explained in the text.

The first corrections to the LO result are suppressed by two powers of the low-momentum scale. The absence of the contributions at order $\nu = 1$ can be traced back to parity conservation which forbids $(\bar{N}N)(\bar{N}N)$ vertices with one spatial derivative and πNN vertices with two derivatives (i. e. $\Delta_i = 1$). The next-to-leading-order (NLO) contributions to the 2NF therefore result from tree diagrams with one insertion of the $\Delta_i = 2$-interaction and one-loop diagrams constructed from the lowest-order vertices, see Fig. 12. The relevant terms in the effective Lagrangian read (147)

$$\begin{aligned}
\mathcal{L}_{\pi}^{(2)} &= \frac{l_3}{16}\langle\chi_+\rangle^2 + \frac{l_4}{16}\Big(2\langle \nabla_\mu U \nabla^\mu U^\dagger\rangle\langle\chi_+\rangle\\
&+ 2\langle \chi^\dagger U \chi^\dagger U + \chi U^\dagger \chi U^\dagger\rangle - 4\langle\chi^\dagger\chi\rangle - \langle\chi_-\rangle^2\Big)\\
&+ \ldots \,,\\
\mathcal{L}_{\pi N}^{(2)} &= \bar{N}\Big(\frac{1}{2\,\mathring{m}}(v\cdot D)^2 - \frac{1}{2\,\mathring{m}} D\cdot D + d_{16} S\cdot u \langle\chi_+\rangle\\
&+ i d_{18} S^\mu [D_\mu, \chi_-] + \ldots \Big) N \,,
\end{aligned}$$

$$\begin{aligned}\mathcal{L}_{NN}^{(2)} &= -\tilde{C}_1\big((\bar{N}DN)\cdot(\bar{N}DN)+((D\bar{N})N)\cdot((D\bar{N})N)\big)\\ &- 2(\tilde{C}_1+\tilde{C}_2)(\bar{N}DN)\cdot((D\bar{N})N)\\ &- \tilde{C}_2(\bar{N}N)\cdot((D^2\bar{N})N+\bar{N}D^2N)+\ldots\,, \qquad (2.12)\end{aligned}$$

where l_i, d_i and $\tilde{C}_i$ denote further LECs and $\mathring{m}$ is the nucleon mass in the chiral limit. The ellipses in the pion and pion-nucleon Lagrangians refer to terms which do not contribute to the nuclear force at NLO. In the case of the nucleon-nucleon Lagrangian $\mathcal{L}_{NN}^{(2)}$ only a few terms are given explicitly. The complete reparametrization-invariant set of terms can be found in (148). The NLO contributions to the two-nucleon potential have been first considered in (149; 150) utilizing the framework of time-ordered perturbation theory. The corresponding energy-independent expressions have been worked out in (151) using the method described in (152) and then re-derived in (142) using an S-matrix-based approach and, independently, in (143; 153) based on the method of unitary transformation. The one-pion (1π) exchange diagrams at NLO do not produce any new momentum dependence. Apart from renormalization of various LECs in Eq. (2.11), one obtains the leading contribution to the Goldberger-Treiman discrepancy (154)

$$\frac{g_{\pi N}}{m}=\frac{g_A}{F_\pi}-\frac{2M_\pi^2}{F_\pi}\,d_{18}+\ldots \qquad (2.13)$$

where the ellipses refer to higher-order terms. Similarly, loop diagrams involving NN short-range interactions only lead to (M_π-dependent) shifts in the LO contact terms. The remaining contributions to the 2NF due to higher-order contact interactions and two-pion exchange have the form:

$$\begin{aligned}V_{\rm 2N}^{(2)} &= -\frac{\boldsymbol{\tau}_1\cdot\boldsymbol{\tau}_2}{384\pi^2F_\pi^4}\,L^{\tilde{\Lambda}}(q)\left(4M_\pi^2(5g_A^4-4g_A^2-1)\right.\\ &+ \left.\vec{q}^{\,2}(23g_A^4-10g_A^2-1)+\frac{48g_A^4M_\pi^4}{4M_\pi^2+\vec{q}^{\,2}}\right)\\ &- \frac{3g_A^4}{64\pi^2F_\pi^4}\,L^{\tilde{\Lambda}}(q)\,\left(\vec{\sigma}_1\cdot\vec{q}\,\vec{\sigma}_2\cdot\vec{q}-\vec{\sigma}_1\cdot\vec{\sigma}_2\,\vec{q}^{\,2}\right)\\ &+ C_1\,\vec{q}^{\,2}+C_2\,\vec{k}^{\,2}+(C_3\,\vec{q}^{\,2}+C_4\,\vec{k}^{\,2})\,\vec{\sigma}_1\cdot\vec{\sigma}_2\\ &+ iC_5\,\frac{1}{2}\,(\vec{\sigma}_1+\vec{\sigma}_2)\cdot\vec{q}\times\vec{k}+C_6\,\vec{q}\cdot\vec{\sigma}_1\,\vec{q}\cdot\vec{\sigma}_2\\ &+ C_7\,\vec{k}\cdot\vec{\sigma}_1\,\vec{k}\cdot\vec{\sigma}_2\,, \qquad (2.14)\end{aligned}$$

where $q\equiv|\vec{q}|$ and the LECs C_i can be written as linear combinations of $\tilde{C}_i$ in Eq. (2.12). The loop function $L^{\tilde{\Lambda}}(q)$ is defined in the spectral function regularization (SFR) (155; 156) as

$$L^{\tilde{\Lambda}}(q)=\theta(\tilde{\Lambda}-2M_\pi)\,\frac{\omega}{2q}\,\ln\frac{\tilde{\Lambda}^2\omega^2+q^2s^2+2\tilde{\Lambda}q\omega s}{4M_\pi^2(\tilde{\Lambda}^2+q^2)}\,, \qquad (2.15)$$

where we have introduced the following abbreviations: $\omega=\sqrt{4M_\pi^2+\vec{q}^{\,2}}$ and $s=\sqrt{\tilde{\Lambda}^2-4M_\pi^2}$. Here, $\tilde{\Lambda}$ denotes the ultraviolet cutoff in the mass spectrum of the two-pion-exchange potential. If dimensional regularization (DR) is employed, the expression for the loop function simplifies to

$$L(q)=\lim_{\tilde{\Lambda}\to\infty}L^{\tilde{\Lambda}}(q)=\frac{\omega}{q}\,\ln\frac{\omega+q}{2M_\pi}\,. \qquad (2.16)$$

In addition to the two-nucleon contributions, at NLO one also needs to consider three-nucleon diagrams shown in the first line of Fig. 13. The first diagram does not involve reducible topologies and, therefore, can be dealt with using the Feynman graph technique. It is then easy to verify that its contribution is shifted to higher orders due to the additional suppression by the factor of $1/m$ caused by the appearance of time derivative at the leading-order $\pi\pi\bar{N}N$ vertex, the so-called Weinberg-Tomozawa vertex. The two remeining diagrams have

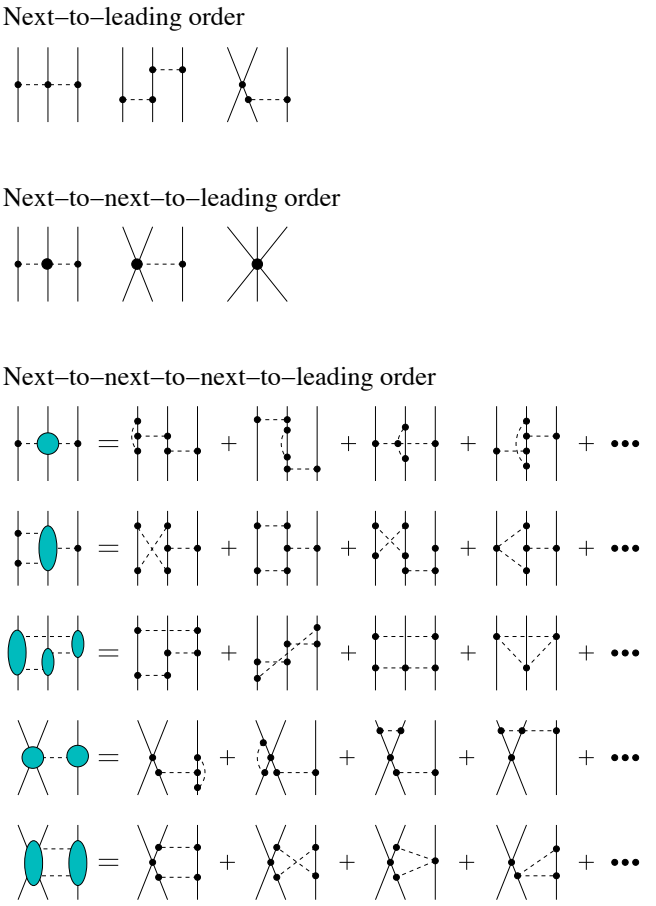

FIG. 13 Chiral expansion of the three-nucleon force up to N^{3}LO. Diagrams in the first line (NLO) yield vanishing contributions to the 3NF if one uses energy-independent formulations as explained in the text. The five topologies at N^{3}LO involve the two-pion exchange, one-pion-two-pion-exchange, ring, contact-one-pion exchange and contact-two-pion-exchange diagrams in order. Shaded blobs represent the corresponding amplitudes. For remaining notation see Fig. 12.

been considered by Weinberg (130; 131) and later by Ordonez and van Kolck (157) using the energy-dependent formulation based on time-ordered perturbation theory. In this approach, it was shown that the resulting 3NF cancels exactly (at the order one is working) against the recoil correction to the 2NF when the latter is iterated in the dynamical equation. In energy-independent approaches such as e.g. the method of unitary transformation which are employed in most of the existing few-nucleon calculations one observes that the irreducible contributions from the last two diagrams in the first line of Fig. 13 are suppressed by the factor $1/m$ and thus occur at higher orders (148), see also (158; 159). Consequently, there is no 3NF at NLO in the chiral expansion.

The contributions at next-to-next-to-leading order ($\mathrm{N^2LO}$) involve one-loop diagrams with one insertion of the subleading vertices of dimension $\Delta_i = 1$, see Fig. 12. The corresponding Lagrangians read:

$$\begin{aligned}\mathcal{L}^{(1)}_{\pi N} &= \bar N\big(c_1\,\langle\chi_+\rangle + c_2\,(v\cdot u)^2 + c_3\,u\cdot u \\ &+ c_4\,[S^\mu,S^\nu]u_\mu u_\nu + c_5\langle\hat\chi_+\rangle\big)N\,, \\ \mathcal{L}^{(1)}_{\pi NN} &= \frac{D}{2}(\bar N N)(\bar N S\cdot u N)\,, \end{aligned} \tag{2.17}$$

where $\hat\chi_+ \equiv \chi_+ - \langle\chi_+\rangle/2$ and D, c_i are the LECs. The 1π-exchange loop diagram again only lead to renormalization of the corresponding LECs. Similarly, the contribution from the last diagram which involves the two-nucleon contact interaction can be absorbed into a redefinition of the LECs $C_{S,T}$ and C_i in Eqs. (2.11), (2.14) (provided one is not interested in the quark mass dependence of the nuclear force). Further, the football diagram yields vanishing contribution due to the antisymmetric (with respect to pion isospin quantum numbers) nature of the Weinberg-Tomozawa vertex. Thus, the only non-vanishing contribution at this order results from the 2π-exchange triangle diagram:

$$\begin{aligned}V^{(3)}_{\rm 2N} &= -\frac{3g_A^2}{16\pi F_\pi^4}\big(2M_\pi^2(2c_1-c_3)-c_3\vec q^{\,2}\big)(2M_\pi^2+\vec q^{\,2}) \\ &\times\; A^{\tilde\Lambda}(q) - \frac{g_A^2 c_4}{32\pi F_\pi^4}\,\boldsymbol{\tau}_1\cdot\boldsymbol{\tau}_2\,(4M_\pi^2+q^2)A^{\tilde\Lambda}(q) \\ &\times\; \big(\vec\sigma_1\cdot\vec q\,\vec\sigma_2\cdot\vec q - \vec q^{\,2}\,\vec\sigma_1\cdot\vec\sigma_2\big)\,, \end{aligned} \tag{2.18}$$

where the loop function $A^{\tilde\Lambda}(q)$ is given by

$$A^{\tilde\Lambda}(q) = \theta(\tilde\Lambda - 2M_\pi)\,\frac{1}{2q}\,\arctan\frac{q(\tilde\Lambda-2M_\pi)}{q^2+2\tilde\Lambda M_\pi}\,. \tag{2.19}$$

In DR, the expression for $A(q)$ takes the following simple form:

$$A(q) \equiv \lim_{\tilde\Lambda\to\infty} A^{\tilde\Lambda}(q) = \frac{1}{2q}\,\arctan\frac{q}{2M_\pi}\,. \tag{2.20}$$

Notice that the triangle diagram also generates short-range contributions which may be absorbed into redefinition of contact interactions. The isoscalar central contribution proportional to the LEC c_3 is attractive and very strong. It is by far the strongest two-pion exchange contribution and reaches a few 10s of MeV (depending on the choice of regularization) at internucleon distances of the order $r \sim M_\pi^{-1}$. The origin of the unnaturally strong subleading 2π-exchange contributions can be traced back to the (numerically) large values of the LECs $c_{3,4}$ and is well understood in terms of resonance exchange related to Δ excitation (160). We will come back to this issue in section II.D where the chiral EFT formulation with explicit Δ degrees of freedom will be discussed. The central 2π-exchange potential was also calculated by Robilotta (161) using the infrared-reglarized version of chiral EFT which enables to sum up a certain class of relativistic corrections (162). He found that the results in the heavy-baryon limit overestimate the ones obtained using infrared regularization by about 25%, see also (163) for a related discussion. Last but not least, the chiral 2π-exchange potential up to $\mathrm{N^2LO}$ has been tested in the Nijmegen partial wave analysis (PWA) of both proton-proton and neutron-proton data (164; 165) where also an attempt has been done to determine the values of the LECs $c_{3,4}$. As demonstrated in these studies, the representation of the (strong) long-range interaction based on the combination of the 1π- and the chiral 2π-exchange potentials rather than on the pure 1π-exchnge potential allows to considerably reduce the number of phenomenological parameters entering the energy-dependent boundary conditions which are needed to parametrize the missing short- and medium-range interactions. Also the extracted values of the LECs $c_{3,4}$ agree reasonably well with various determinations in the pion-nucleon system. These studies provide a beautiful confirmation of the important role of the 2π-exchange potential in nucleon-nucleon scattering observables, see, however, Ref. (166) for a criticism. For a similar work utilizing the distorted-wave methods the reader is referred to (167; 168).

The first nonvanishing contributions to the 3NF also show up at $\mathrm{N^2LO}$ and arise from tree diagrams shown in Fig. 13 which involve a single insertion of the subleading vertices $\mathcal{L}^{(1)}$ in Eq. (2.17) and

$$\mathcal{L}^{(1)}_{NNN} = -\frac{1}{2}(\bar N N)(\bar N\boldsymbol{\tau}N)\cdot(\bar N\boldsymbol{\tau}N)\,. \tag{2.21}$$

where E is a low-energy constant. The corresponding 3NF expression read:

$$\begin{aligned}V^{(3)}_{3N} &= \frac{g_A^2}{8F_\pi^4}\,\frac{\vec\sigma_1\cdot\vec q_1\,\vec\sigma_3\cdot\vec q_3}{[q_1^2+M_\pi^2]\,[q_3^2+M_\pi^2]}\,\Big[\boldsymbol{\tau}_1\cdot\boldsymbol{\tau}_3\,\big(-4c_1M_\pi^2 \\ &\quad + 2c_3\,\vec q_1\cdot\vec q_3\big) + c_4\boldsymbol{\tau}_1\times\boldsymbol{\tau}_3\cdot\boldsymbol{\tau}_2\,\vec q_1\times\vec q_3\cdot\vec\sigma_2\Big] \\ &- \frac{g_A\,D}{8F_\pi^2}\,\frac{\vec\sigma_3\cdot\vec q_3}{q_3^2+M_\pi^2}\,\boldsymbol{\tau}_1\cdot\boldsymbol{\tau}_3\,\vec\sigma_1\cdot\vec q_3 \\ &+ \frac{1}{2}E\,\boldsymbol{\tau}_2\cdot\boldsymbol{\tau}_3\,, \end{aligned} \tag{2.22}$$

where the subscripts refer to the nucleon labels and $\vec q_i = \vec p_i\,' - \vec p_i$, with $\vec p_i\,'$ and $\vec p_i$ being the final and initial

momenta of the nucleon i. The expressions in Eq. (2.22) correspond to a particular choice of nucleon labels. The full expression for the 3NF results by taking into account all possible permutations of the nucleons (for three nucleons there are altogether six permutations), i.e.:

$$V_{\rm 3N}^{\rm full} = V_{\rm 3N} + \text{all permutations}\,. \qquad (2.23)$$

We further emphasize that the expressions for the 3NF given in Refs. (157; 169) contain one redundant 1π-exchange and two redundant contact interactions. As shown in (123), only one independent linear combination contributes in each case if one considers matrix elements between antisymmetrized few-nucleon states, see also (92) for a related discussion.

We now turn to next-to-next-to-next-to-leading order ($\mathrm{N^3LO}$) and discuss first the corrections to the 2NF. As follows from Eq. (2.8), one has to account for contributions from tree diagrams with one insertion from $\mathcal{L}^{(4)}$ or two insertions from $\mathcal{L}^{(2)}$, one-loop diagrams with one insertion from $\mathcal{L}^{(2)}$ or two insertions from $\mathcal{L}^{(1)}$ as well as two-loop graphs constructed from the lowest-order vertices, see Fig. 12. Apart from renormalization of various LECs, the 1π-exchange potential receives at this order (in the scheme based on the counting $m \sim \mathcal{O}(\Lambda^2/M_\pi)$) the first relativistic corrections proportional to m^{-2}. These are scheme-dependent and have to be chosen consistently with the $1/m$-corrections to the 2π-exchange potential and the relativistic extension of the dynamical equation, see (170) for a comprehensive discussion. The two-pion exchange contributions at $\mathrm{N^3LO}$ were worked out by Kaiser (171) based on the one-loop representation of the πN scattering amplitude. We refrain from giving here the rather involved expressions for the sub-subleading 2π-exchange potential and refer to the original work (171) where the results are given in terms of the corresponding spectral functions. For certain classes of contributions, the integrals over the two-pion exchange spectrum could be performed analytically and are given in Ref. (172). Notice further that the subleading (i.e. the ones proportional to m^{-2}) relativistic corrections of the 2π-exchange range have also been worked out by Kaiser (173). In the counting scheme with $m \sim \mathcal{O}(\Lambda^2/M_\pi)$, these terms, however, would only appear at $\mathrm{N^5LO}$. It should also be emphasized that the $\mathrm{N^3LO}$ contributions to the 2π-exchange potential were worked out in the covariant version of chiral EFT (more precisely, using the formulation by Becher and Leutwyler (162)) by Higa et al. (174–176).

3π-exchange contributions also appear at this order in the chiral expansion and have been worked out in Refs. (177; 178), see also Ref. (179) for a related work. The resulting potentials turn out to be rather weak. For example, the strongest contribution is of the isoscalar spin-spin type (i.e. proportional to $\vec\sigma_1\cdot\vec\sigma_2$) and about 10 times weaker than the corresponding 2π-exchange contribution at the same order at relative distances $r \sim M_\pi^{-1}$. It should, however, be emphasized that the subleading 3π-exchange contributions at $\mathrm{N^4LO}$ are larger in size (180) which, again, can be traced back to the large values of the LECs c_i. Finally, the last type of the 2NF corrections at this order results from diagrams involving contact interactions. The most general polynomial (in momenta) representation of the short-range part of the potential involves, apart from the two leading and seven subleading terms given in Eqs. (2.11) and (2.14) fifteen new contact interactions (in the isospin invariant sector) yielding in total 24 LECs to be determined from nucleon-nucleon data.

The 3NF contributions at $\mathrm{N^3LO}$ feed into five different topologies, see Fig. 13, and are currently being worked out. Currently, the expressions for the first three topologies which do not involve short-range contact interactions are available. The one-loop corrections to the 2π-exchange diagrams can, to a large extent, be accounted for by a finite shift $c_i \to \bar c_i = c_i + \delta c_i$ of the LECs c_i (181; 182)

$$\delta c_1 = -\frac{g_A^2\, M_\pi}{64\pi F_\pi^2}\,, \qquad \delta c_3 = -\delta c_4 = \frac{g_A^4\, M_\pi}{16\pi F_\pi^2}\,. \qquad (2.24)$$

Numerically, these corrections are of the order of 20% of the corresponding LECs and are consistent with the difference in values of c_i between the order-Q^2 and Q^3 determinations from the pion-nucleon system, see (160; 183–185). The only 2π-exchange contribution that cannot be cast into redefinition of the LECs c_i arises from the diagram which involves pions interacting in flight, see (181; 182) for the explicit expression. We also emphasize that there are no 2π-exchange contributions from tree diagrams with one insertion from $\mathcal{L}^{(2)}_{\pi N}$ in Eq. (2.12) (except for the relativistic corrections). This is because diagrams involving subleading πNN interaction do not yield any irreducible contributions while the ones with the $\pi\pi NN$-vertices of dimension $\nu = 2$ involve at least one time derivative and are, therefore, suppressed by a factor of $1/m$. This observation is consistent with the absence of logarithmic ultraviolet divergences in the loop diagrams. In this context, it should be emphasized that the requirement of renormalizability at $\mathrm{N^3LO}$ (and, presumably, also at higher orders) was found to impose strong constraints on the unitary ambiguity in the form of the resulting nuclear potentials. This issue is discussed extensively in (186) and may remind one of the recent findings in the context of large-N_c QCD (187–189) where it was shown that the multiple-meson-exchange potential derived in the energy-dependent formulation is inconsistent with large-N_C counting rules. The consistency could be maintained using a different (but equivalent up to the considered order) form of the potential based on the energy-independent formalism, see Ref. (189) for more details. The contributions from the two-pion-one-pion exchange and ring diagrams are given explicitly in Ref. (181) where expressions are shown both in momentum and coordinate spaces. Especially in the case of ring diagrams where loop integrals involve two independent external momenta and, therefore, yield rather involved expressions in momentum space. It is advantageous to switch to coordinate space where a much more compact

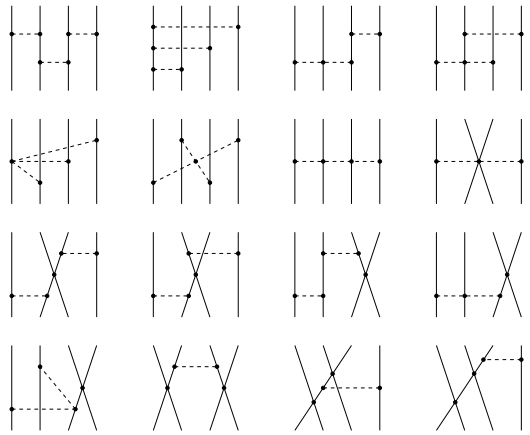

FIG. 14 Diagrams contributing to the four-nucleon force at N^{3}LO. For notation see Fig. 12.

representation emerges. Notice further that ring diagrams were already studied in the pioneering work (190). The calculation of the last two topologies involving the leading contact interactions is in progress. Last but not least, one should also take into account the leading relativistic $1/m$-corrections to the NLO three-nucleon diagrams, see the first line in Fig. 13. Again, these contributions are scheme-dependent and should be chosen consistently with the relativistic corrections to the 2NF and the form of the dynamical equation. The $1/m$-corrections to the 2π-exchange 3NF have already been worked out long time ago by Coon and Friar and are given in the most general form in Ref. (158). Notice further that at this order, one needs to account for the dependence of the 2NF on the total momentum of the 2N system (effects due to drift of the CMS of a two-body subsystem). Such boosted 2N operators may, in fact, also be viewed as 3N operators. In the context of chiral EFT, this kind of corrections is discussed in (191).

The last type of N^{3}LO contributions arises from four-nucleon tree diagrams constructed from the lowest-order vertices, see in Fig. 14, which have been evaluated recently using the method of unitary transformation (186; 192). Notice that the first two diagrams in the second line were already discussed long ago, see e.g. (193; 194). Furthermore, it should be emphasized that disconnected diagrams calculated e.g. in (169) using time-ordered perturbation theory do not contribute to the nuclear force in the method of unitary transformation. It has been conjectured in Ref. (194) that 4N diagrams which involve reducible topologies do not generate irreducible pieces in the amplitude and thus lead to vanishing 4NFs. While this is indeed the case for the leading 3N diagrams at NLO, it is explicitly shown in Ref. (186; 192) that many of the reducible-like diagrams in Fig. 14 do generate non-vanishing 4NFs which are not suppressed by inverse powers of the nucleon mass. As a representative example, we give here the g_A^6-contribution which results entirely from the first diagram in Fig. 14 (the second graph appears to be truly reducible and does not produce any contribution to the 4NF):

$$\begin{aligned} V_{4N}^{(4)} &= -\frac{2g_A^6}{(2F_\pi)^6}\frac{\vec\sigma_1\cdot\vec q_1\;\vec\sigma_4\cdot\vec q_4}{[\vec q_1^{\,2}+M_\pi^2]\,[\vec q_{12}^{\,2}+M_\pi^2]^2\,[\vec q_4^{\,2}+M_\pi^2]} \\ &\times\Big[(\boldsymbol\tau_1\cdot\boldsymbol\tau_4\,\boldsymbol\tau_2\cdot\boldsymbol\tau_3-\boldsymbol\tau_1\cdot\boldsymbol\tau_3\,\boldsymbol\tau_2\cdot\boldsymbol\tau_4)\,\vec q_1\cdot\vec q_{12}\,\vec q_4\cdot\vec q_{12} \\ &+\boldsymbol\tau_1\times\boldsymbol\tau_2\cdot\boldsymbol\tau_4\;\vec q_1\cdot\vec q_{12}\;\vec q_{12}\times\vec q_4\cdot\vec\sigma_3 \\ &+\boldsymbol\tau_1\times\boldsymbol\tau_3\cdot\boldsymbol\tau_4\;\vec q_4\cdot\vec q_{12}\;\vec q_1\times\vec q_{12}\cdot\vec\sigma_2 \\ &+\boldsymbol\tau_1\cdot\boldsymbol\tau_4\;\vec q_{12}\times\vec q_1\cdot\vec\sigma_2\;\vec q_{12}\times\vec q_4\cdot\vec\sigma_3\Big]+\text{all perm.}, \end{aligned} \tag{2.25}$$

where $\vec q_{12}=\vec q_1+\vec q_2=-\vec q_3-\vec q_4=-\vec q_{34}$ is the momentum transfer between the nucleon pairs 12 and 34. The complete expression for the leading 4NF both in momentum and coordinate space can be found in Ref. (186). A rough estimation of the 4NF contributions to e.g. the α-particle binding energy is provided by the strength of the corresponding r-space potentials expressed in terms of dimensionless variables $r_{ij}M_\pi$. One then finds e.g. for the g_A^6-terms $g_A^6M_\pi^7(16\pi F_\pi^2)^{-3}\sim 50$ keV. This agrees qualitatively with a more accurate numerical estimation carried out in Ref. (195) which, however, still involved severe approximations to simplify the calculations.

So far we only discussed isospin-invariant contributions to the nuclear forces. It is well established that nuclear forces are charge dependent (for reviews see e.g. (196; 197)). For example, in the nucleon-nucleon $^1S_0$ channel one has for the scattering lengths a and the effective ranges r (after removing electromagnetic effects)

$$\begin{aligned} a_{\rm CIB} &= \frac{1}{2}\,(a_{nn}+a_{pp})-a_{np}=5.64\pm0.40\ \text{fm}\,, \\ r_{\rm CIB} &= \frac{1}{2}\,(r_{nn}+r_{pp})-r_{np}=0.03\pm0.06\ \text{fm} \end{aligned} \tag{2.26}$$

These numbers for charge independence breaking (CIB) are taken from the recent compilation of Machleidt (18). The charge independence breaking in the scattering lengths is large, of the order of 25%, since $a_{np}=(-23.740\pm0.020)$ fm. Of course, it is magnified at threshold due to kinematic factors (as witnessed by the disappearance of the effect in the effective range). In addition, there are charge symmetry breaking (CSB) effects leading to different values for the pp and nn phase shifts/threshold parameters,

$$\begin{aligned} a_{\rm CSB} &= a_{pp}-a_{nn}=1.6\pm0.6\ \text{fm}\,, \\ r_{\rm CSB} &= r_{pp}-r_{nn}=0.10\pm0.12\ \text{fm}\,. \end{aligned} \tag{2.27}$$

Combining these numbers gives as central values $a_{nn}=-18.9$ fm and $a_{pp}=-17.3$ fm. Notice that this value for a_{nn} is in agreement with the recent experimental determinations from the reaction $\pi^-d\to nn\gamma$, $a_{nn}=-18.5\pm0.5$ fm (198), and the kinematically complete deuteron breakup reaction $nd\to nnp$ at $E_{\rm lab}=13$ MeV, $a_{nn}=-18.7\pm0.6$ fm (199). However, another recent experiment also based on the deuteron breakup reaction

at $E_{\rm lab} = 25.2$ MeV yielded a considerably smaller value, $a_{nn} = -16.3 \pm 0.4\,$fm (200). For a review of indirect methods to measure the ${}^1S_0$ nn scattering length and the current experimental status for this observable see (201).

Within the Standard Model, isospin violation has its origin in the different masses of the up and down quarks and the electromagnetic interactions. Chiral EFT is well suited to explore the consequences of these two effects for low-energy dynamics of few- and many-nucleon systems. Consider first the strong isospin-violating effects. The QCD quark mass term can be written in the two-flavor case as

$$\mathcal{L}^{\rm QCD}_{\rm mass} = -\frac{1}{2}\bar{q}(m_u + m_d)(1 + \epsilon\tau^3)q\,, \qquad (2.28)$$

where the superscript of the Pauli isospin matrix denotes the corresponding Cartesian component and

$$\epsilon \equiv \frac{m_u - m_d}{m_u + m_d} \sim -\frac{1}{3}\,. \qquad (2.29)$$

Here, the numerical estimation corresponds to the modified $\overline{\rm MS}$ subtraction scheme at a renormalization scale of 1 GeV (202). In Eq. (2.28), the isoscalar term breaks chiral but preserves isospin symmetry. It is responsible e.g. for the nonvanishing pion mass $M^2 = (m_u + m_d)B$, $M_\pi^2 = M^2 + \mathcal{O}(m_{u,d}^2)$, and generates a string of chiral-symmetry-breaking terms in the effective hadronic Lagrangian proportional to M^{2n} with $n = 1, 2, \ldots$. The isovector term gives rise to the strong isospin breaking and leads to hadronic effective interactions $\propto (\epsilon M^2)^n$. Consequently, the typical size of the strong isospin violation in hadronic observables is given by $\epsilon M_\pi^2/\Lambda^2 \sim 1\%$ if one takes $\Lambda = M_\rho$ (this, however, does not apply e.g. to the pion masses). The leading and subleading strong isospin-violating contributions are already incorporated in the Lagrangians $\mathcal{L}_\pi^{(2)}$ and $\mathcal{L}_{\pi N}^{(1,2)}$ in Eqs. (2.9), (2.12), (2.17) and correspond to terms involving χ, $\chi_\pm$. Notice that the strong isospin violation is additionally suppressed in the meson sector (due to G-parity). In particular, the charged-to-neutral pion mass difference is almost entirely of electromagnetic origin. Electromagnetic terms in the effective Lagrangian resulting from exchange of hard virtual photons can be generated using the method of external sources (35). All such terms are proportional to positive powers of the nucleon charge matrix $Q = e(1+\tau^3)/2$ where e denotes the electric charge. In addition, soft photons have to be included explicitly. For more details on the inclusion of virtual photons in chiral EFT the reader is referred to (203–209).

To explore isospin-breaking (IB) effects in nuclear forces/few-nucleon observables it is useful to relate the corresponding small parameters ϵ and e to the chiral expansion parameter M_π/Λ. Clearly, this can be done in various ways. For example, in Refs. (210–212) the following rules have been adopted:

$$\epsilon \sim e \sim \frac{M_\pi}{\Lambda}; \qquad \frac{e^2}{(4\pi)^2} \sim \frac{M_\pi^4}{\Lambda^4}\,. \qquad (2.30)$$

Similar counting rules were also used in Refs. (213–218). Notice, however, that in the meson and single-baryon sectors one usually counts $\epsilon \sim 1$ but $e \sim M_\pi/\Lambda$. Utilizing the counting rules in Eq. (2.30), the leading and subleading IB contributions from the hard virtual photons have the form (208):

$$\begin{aligned}
\mathcal{L}^{(2)}_{\pi,\,\rm em} &= C\langle QUQU^\dagger\rangle\,,\\
\mathcal{L}^{(3)}_{\pi N,\,\rm em} &= F^2\bar{N}\big(f_1\langle\tilde{Q}_+^2 - \tilde{Q}_-^2\rangle + f_2\langle Q_+\rangle\tilde{Q}_+\\
&\quad + f_3\langle\tilde{Q}_+^2 + \tilde{Q}_-^2\rangle\big)N\,, \qquad (2.31)
\end{aligned}$$

where $\tilde{Q}_\pm \equiv Q_\pm - 1/2\langle Q_\pm\rangle$ and f_i refer to the corresponding LECs. The leading Lagrangians for the strong and electromagnetic IB contact interactions $\mathcal{L}^{(3)}_{NN,\,\rm str}$ and $\mathcal{L}^{(4)}_{NN,\,\rm em}$ are given explicitly in Ref. (210).

Let us first discuss IB contributions to the pion and nucleon masses. As already pointed out, the leading contribution to the charged–to–neutral pion mass difference is entirely of electromagnetic origin,

$$\delta M_\pi^2 \equiv M_{\pi^\pm}^2 - M_{\pi^0}^2 \simeq \frac{2}{F^2}e^2C\,. \qquad (2.32)$$

The experimentally known pion mass difference $M_{\pi^\pm} - M_{\pi^0} = 4.6$ MeV allows to fix the value of the LEC C, $C = 5.9\cdot 10^{-5}$ GeV^4. Notice that the natural scale for this LEC is $F_\pi^2\Lambda^2/(4\pi)^2 \sim 3\cdot 10^{-5}$ GeV^4 if one adopts $\Lambda \sim M_\rho$. Writing the nucleon mass m as

$$m \equiv {\rm diag}(m_p,\ m_n) = m + \frac{1}{2}\delta m\,\tau^3\,, \qquad (2.33)$$

one obtains for the proton-to-neutron mass difference δm:

$$\delta m = -4c_5\epsilon M_\pi^2 - f_2\,e^2F_\pi^2 + \ldots\,, \qquad (2.34)$$

where the ellipses refer to higher-order corrections. Notice that the f_3-term in Eq. (2.31) is isospin-invariant. On the other hand, the f_1-term does produce IB vertices with two and more pions but does not contribute to the leading electromagnetic nucleon mass shift. The LECs c_5 and f_2 can be determined from the strong and electromagnetic nucleon mass shifts:

$$\begin{aligned}
(m_p - m_n)^{\rm str} &= (\delta m)^{\rm str} = -2.05 \pm 0.3\ \text{MeV}\,,\\
(m_p - m_n)^{\rm em} &= (\delta m)^{\rm em} = 0.76 \pm 0.3\ \text{MeV}\,, \qquad (2.35)
\end{aligned}$$

which leads to (207)

$$c_5 = -0.09 \pm 0.01\ \text{GeV}^{-1}\,, \quad f_2 = -0.45 \pm 0.19\ \text{GeV}^{-1}\,.$$

The values for the strong and electromagnetic nucleon mass shifts are taken from (219). Notice that the recent lattice QCD result (220) for the strong nucleon mass shift $(\delta m)^{\rm str} = -2.26 \pm 0.57 \pm 0.42 \pm 0.10$ MeV is in agreement with the one of Ref. (219). We further emphasize that according to the counting rules in Eq. (2.30), the electromagnetic contribution to the nucleon mass shift is formally of higher order than the strong one. Based on

naive dimensional analysis, these contributions are expected to be of the size $|(\delta m)^{\rm str}| \sim \epsilon M_\pi^2/M_\rho \sim 8$ MeV and $|(\delta m)^{\rm em}| \sim e^2 M_\rho/(4\pi)^2 \sim 0.5$ MeV.

We are now in the position to overview the structure of the IB nuclear forces. The general isospin structure of the two-nucleon force feeds, according to the classification of Henley and Miller (221), into the four classes: $V_{2N}^I = \alpha + \beta\,\boldsymbol{\tau}_1\cdot\boldsymbol{\tau}_2$ (isospin-invariant), $V_{2N}^{II} = \alpha\,\tau_1^3\tau_2^3$ (charge-independence-breaking), $V_{2N}^{III} = \alpha\,(\tau_1^3+\tau_2^3)$ (charge-symmetry-breaking) and $V_{2N}^{IV} = \alpha\,(\tau_1^3-\tau_2^3)+\beta\,[\boldsymbol{\tau}_1\times\boldsymbol{\tau}_2]^3$ (issospin-mixing). Here, α and β denote the corresponding space and spin operators. Notice that for the class-IV terms, β has to be odd under a time reversal transformation. The most general isospin structure of the 3NF is worked out in Ref. (211). While the distinction between the class-I, II and III forces based on the conservation of the total isospin operator $\boldsymbol{T} = (\sum_i \boldsymbol{\tau}_i)/2$ and charge-symmetry operator $P_{cs} = \exp(i\pi T_2)$ can be straightforwardly generalized to any number of nucleons, the conservation of the operator $\boldsymbol{T}^2$ responsible for the distinction between the class-III and IV 2NFs depends, in general, on the number of nucleons. In particular, the class-II and III 2NFs commute with the operator $\boldsymbol{T}_{2N}^2$ (i.e. do not mix isospin in the 2N system) but do not commute with $\boldsymbol{T}_{>2N}^2$. For this reason, the general isospin structure of the 3NF was classified in Ref. (211) in terms of class-I, II and III contributions.

The dominant IB contribution to the 2NF occurs at NL$\not{0}$ (the slash indicates that we now use the power counting rules extended as in Eq. (2.30)) due to the charge-to-neutral pion mass difference in the 1π-exchange potential. It can be accounted for by taking the proper pion masses in the 1π-exchange potential for various physical channels:

$$\begin{aligned} V_{1\pi}^{pp} &= V_{1\pi}^{nn} = V_{1\pi}(M_{\pi^0})\,, \\ V_{1\pi}^{np} &= -V_{1\pi}(M_{\pi^0}) + 2(-1)^{I+1} V_{1\pi}(M_{\pi^\pm})\,, \end{aligned} \tag{2.36}$$

where I denotes the total isospin of the two-nucleon system and

$$V_{1\pi}(M_{\pi^\pm}) = -\frac{g_A^2}{4F_\pi^2}\frac{\vec\sigma_1\cdot\vec q\,\vec\sigma_2\cdot\vec q}{\vec q^{\,2}+M_\pi^2}\,. \tag{2.37}$$

Notice that the resulting IB interaction conserves charge symmetry (i.e. class-II) and reaches about $\delta M_\pi^2/M_\pi^2 \sim 7\%$ of the strength of the isospin-invariant 1π-exchange potential. It is known to yield a sizeable contribution to the CIB in the $^1S_0$ NN scattering length, see e.g. (210). Another IB effect at the same order comes from the Coulomb interaction between the protons (class-II and III). We emphasize that effects of the purely electromagnetic interactions in two-nucleon scattering observables get enhanced under certain kinematical conditions (low energies and/or forward angles) due to the long-range nature of these interactions. Clearly, such an enhancement goes beyond the simple power counting rules in Eq. (2.30). Consequently, despite the fact that the first corrections to the point-like static one-photon exchange (Coulomb interaction) due to recoil and two-photon exchange (222), pion loop contributions to the nucleon form factors (223), vacuum polarization (224; 225) and magnetic moment interaction (226) are suppressed by the factor $1/m^2$ and, according to the power counting, contribute at rather high orders, sizeable effects may show up in certain observables. For example, the magnetic moment interaction strongly affects the nucleon analyzing power A_y at low energy and forward angles. Effects of subleading electromagnetic interactions were also investigated in 3N continuum using phenomenological nuclear forces (227; 228), see (229) for a formulation based on pionless EFT.

The corrections to the IB 2NF at N^{2}L$\not{0}$ are CSB and arise from charge dependence of the pion-nucleon coupling constant in the 1π-exchange potential and the derivative-less NN contact interaction $\propto m_u - m_d$ (212; 214). Notice, however, that the energy-dependent Nijmegen PWA does not yield any evidence for charge dependence of the pion-nucleon coupling constant (230). The leading CIB contact interactions are of electromagnetic origin and (formally) start to contribute at N^{3}L$\not{0}$. At this order, one also has to take into account further IB contributions to the 1π-exchange potential at the one-loop level which, to a large extent, can be accounted for by a further (charge-dependent) renormalization of the πN coupling constants in Eq. (2.36). The only contributions which have a different momentum dependence and, therefore, cannot be cast into the form of Eq. (2.36) are the ones $\propto (\delta M_\pi)^2$ and the proton-to-neutron mass difference which involve class-IV operators (212; 217), see (231) for a much earlier derivation of these terms. Notice that the power counting rules in Eq. (2.30) suggests the following hierarchy of the 2NF (213): $V_{2N}^I > V_{2N}^{II} > V_{2N}^{III} > V_{2N}^{IV}$ which is consistent with the observations. Next, $\pi\gamma$-exchange also contributes at this order. The resulting CIB potential has been worked out by van Kolck at al. (232) and re-derived recently by Kaiser (223). It can be written in a rather compact way and leads to negligibly small effects in NN scattering. Kaiser also calculated subleading contributions to the $\pi\gamma$-exchange potential proportional to the large isovector magnetic moment $\kappa_v = 4.7$ of the nucleon and found that the resulting potentials, which are also CIB, have a similar strength as the leading-order one (223).[#4] IB 2π-exchange also starts to contribute at N^{3}L$\not{0}$ and is driven by the neutral-to-charged pion mass difference (CIB) (215) and the strong contribution to the nucleon mass shift (CSB) (212; 216; 233; 234), see (210) for the application to NN phase shifts. Finally, there are also the first IB 3NFs. While the dominant CIB 2π-exchange 2NF is generated by the pion mass difference,

[#4] Notice, however, that these corrections are suppressed by the factor $1/m$ relative to the leading-order contributions and, therefore, appear formally at N^{5}L$\not{0}$.

the 3N diagrams with one insertion of δM_π^2 at $\mathrm{N^3LO}$ are additionaly suppressed by the factor $1/m$ (if one uses an energy-independent formulation), see the discussion about the 3NFs at NLO earlier in the text. The nonvanishing 3NFs at $\mathrm{N^3LO}$ result from 1π- and 2π-exchange 3N diagrams constructed with the leading-order isospin-invariant vertices and a single insertion of δm as well as 2π-exchange diagram with the leading IB $\pi\pi NN$ interactions $\propto f_{1,2}$ (211; 218). One finds that all these contributions are CSB except the one which is proportional to LEC f_1 and is CIB. We further emphasize that while the value of the LEC f_2 is determined by the electromagnetic nucleon mass shift, the value of the LEC f_1 is unknown. However, see (209) for an estimation of f_1 based on dimensional analysis and (235) for an attempt to determine f_1 from data.

Remarkably, even the $\mathrm{N^4LO}$ contributions to the two- and three-nucleon forces have been worked out. At this order, no new structures appear in the 1π-exchange potentials. The corrections to the leading IB 2π-exchange potential result from a single insertion of either the subleading isospin-conserving $\pi\pi NN$ vertices proportional to the LECs c_i, see Eq. (2.17), the leading electromagnetic vertex proportional to the LEC f_2, see Eq. (2.31), [#5] or the (poorly known) leading charge-dependance of the pion-nucleon coupling constant (212). The resulting IB potentials involve the class-II and III central, tensor and spin-spin components. The CIB potentials typically have the strength of a few 10 keV at relative distances $r \sim M_\pi^{-1}$. The CSB tensor and spin-spin potentials are weaker (< 10 keV) while the CSB central potential is comparable in size to the CIB contributions. Similarly to the isospin-conserving 2π-exchange potential, the subleading contributions turn out to be numerically large in comparison to the leading-order ones. In particular, for the class-III central 2π-exchange potential one obtains $V_{2N}^{2\pi,\,(5)}/V_{2N}^{2\pi,\,(4)} \simeq 3$ for $r \sim M_\pi^{-1}$. The main reason for this unpleasant convergence pattern is the same as in the isospin-conserving case and can be traced back to the (large) Δ-isobar contributions to the LECs $c_{3,4}$. We will discuss this issue in more detail in section II.D. Last but not least, there are also numerous IB contact interactions with up to two derivatives involving class-II, III and IV terms, see also (217). The corrections to the 3NF at $\mathrm{N^4LO}$ are worked out in Refs. (211; 218). At this order, the first IB but charge symmerty conserving 3NFs show up which result from the neutral-to-charged pion mass difference in the $\mathrm{N^2LO}$ 2π- and 1π-exchange diagrams in the second line of Fig. 13 and the 2π-exchange diagram involving the $\pi\pi NN$ vertex $\propto f_1$. In addition, there are CSB 3NFs of the 2π- and 1π-exchange types driven by the electromagnetic nucleon mass shift. Again, the strongest 3NFs turn out to be the ones which are proportional to the LECs $c_{3,4}$. They are charge-symmetry conserving and arise from a single insertion of δM_π^2 into the pion propagators of the 2π-exchange 3N graph. The expected strength of such IB potentials is $\sim 2\delta M_\pi^2/M_\pi^2 \sim 13\,\%$ as compared to the isospin-invariant ones given in Eq. (2.22) which are known to yield about $\sim 500\ldots1000$ keV to the triton binding energy (the precise numbers are renormalization scheme dependent). Also the strength of the corresponding coordinate-space potentials, e.g. $|g_A^2 \delta M_\pi^2 M_\pi^4 c_3/(64\pi^2 F_\pi^4)| \sim 70$ keV (here we picked out one particular term), indicates that the resulting IB effects in few-nucleon observables might be sizeable. The CSB 3NFs, on the other hand, do show a more natural convergence pattern and are considerably waeker. Their contribution to e.g. the ^{3}H-^{3}He binding energy difference is expected to be of the order ~ 10 keV.

Recently, a certain classes of even higher-order contributions have been worked out by Kaiser. In particular, he calculated the subleading $\pi\pi\gamma$-exchange potentials proportional to the LECs $c_{3,4}$ at the 2-loop level which (formally) contribute at order $\mathrm{N^6LO}$ (236; 237). Especially the contributions driven by the LEC c_3 were found to generate astonishingly strong CSB and CIB potentials which amount to $\sim 1\%$ of the strongly attractive isoscalar central potential at $\mathrm{N^2LO}$ and reach a few 100s of keV at $r \sim M_\pi^{-1}$. Notice, however, that effects of these very strong potentials in S-, P- and D-waves may, to some extent, be compensated by the corresponding IB contact interactions. The effects in higher partial waves are presumably suppressed due to the shorter range of the 2π-exchange potential compared with the 1π-exchange one.

C. Chiral EFT for few nucleons: applications

We now turn our attention to applications. As discussed in the previous section, the two-nucleon chiral potential involves the long-range contributions due to the multiple pion exchanges and short-range ones parametrized by contact interactions. Both kinds of terms typically grow with increasing nucleon momenta and become meaningless in the large-momentum region as follows from the very nature of EFT being the low-momentum expansion. As a consequence, the Schrödinger equation is ultraviolet divergent and needs to be regularized (and renormalized). The problem of renormalization in the nonperturbative regime in the context of both pion-less (41; 238–245) and pion-full EFT (139; 140; 168; 246–266) has attracted a lot of interest in the past years. The standard procedure to renormalize the Lippmann-Schwinger (LS) equation is based on Wilson's method and implies the following two steps (246). First, one solves the LS equation regularized with the finite momentum (or coordinate-space) cutoff and using the potential truncated at a given order in the chiral expansion as the kernel. Secondly, the LECs accompany-

[#5] The two other LECs $f_{1,3}$ do not contribute to the 2π-exchange 2NF at this order.

ing the contact terms in the potential are determined by matching the resulting phase shifts to experimental data which, in this framework, can be viewed as renormalization. Notice that iterating the *truncated* expression for the chiral potential in the LS equation necessarily generates ultraviolet divergencies in the Neumann series which require counterterms beyond the given approximation for the potential. As a consequence, taking the limit of the infinite cutoff in such a manifestly non-renormalizable (in the above mentioned sense) approach might result e.g. in impossibility to resolve the (nonlinear) matching conditions for the corresponding LECs. A detailed discussion on the choice of ultraviolet cutoff and its role in renormalization of the Schrödinger equation is given by Lepage (246; 247). He argued that the coordinate-space (momentum-space) cutoff should not be decreased (increased) beyond the separation scale, after which the description of the data stops to improve. Taking the cutoff near this separation scale is the most efficient choice. This strategy has been followed by the currently most advanced N^{3}LO analyses of the 2N system of Refs. (271; 272) where the cutoffs $\Lambda = 450 \ldots 600$ MeV have been employed. These studies were critisized by Nogga et al. (139) who considered low NN partial waves based on the 1π-exchange potential and contact interactions using a much bigger cutoff variation with $\Lambda < 4$ GeV. They found that higher-order counterterms have to be promoted to LO in the $^3P_0$, $^3P_2$-$^3F_2$ and $^3D_2$ channels in order to stabilize the amplitude. On the other hand, the efficiency of such a modified power counting framework was questioned in Ref. (258), where it has been demonstrated that increasing the cutoff and promoting counterterms as suggested in Ref. (139) does not improve the overall description of the scattering observables. For more discussions on the conceptual issues related to the power counting in the NN system the reader is referred to (139; 140; 168; 246; 247; 254; 258; 262). More work is needed in the future in order to clarify the relation between the well-established chiral expansion of the nuclear potential and the scattering amplitude.

We further emphasize that it is possible to *nonperturbatively* renormalize the partial-wave-projected LS equation with singular $1/r^n$-potentials (112; 262; 267–270). This program was applied to different NN channels based on the 1π- and 2π-exchange potentials at various orders in the chiral expansion by the Granada group (252; 253; 255–257; 260; 263; 264). In these studies, the short-range counter terms are replaced by adjustable parameters entering the short-distance boundary conditions. The number of such parameters in each channel is uniquely determined by the sign (attractive vs. repulsive) of the strongest singularity which raises concerns about a systematic improvability (in the EFT sense) of such a framework. Nevertheless, the findings of these studies in attractive channels provide an impressive demonstration of the existence of the long-range correlations in the NN scattering observables.

The most advanced analyses of the two-nucleon system based on the Weinberg power counting take into account the 2NF contributions up to N^{3}LO (271; 272). Most of the LECs c_i, d_i entering the long-range part of the potential are sufficiently well determined in the pion-nucleon system (184).[#6] The 24[#7] unknown LECs entering the short-range part of the 2NF at N^{3}LO have been extracted from the low-energy NN data for several choices of the cutoff in the Schrödinger equation. Both N^{3}LO potentials of Entem and Machleidt (271) (EM) and Epelbaum, Glöckle and Meißner (272) (EGM) yield accurate results for the neutron-proton phase shifts up to $E_{\rm lab} \sim 200$ MeV and the deuteron observables. This is exemplified in Figs. 15, 16 where the EGM and EM results for the neutron-proton S- P- and D-waves and the corresponding mixing angles are shown in comparison with PWA results from Refs. (273–275). The bands in the EGM analysis result from the variation of the cutoff in the LS equation (spectral function regularization) in the range $\Lambda = 450 \ldots 600$ MeV ($\tilde{\Lambda} = 500 \ldots 700$ MeV). It is comforting to see that in most cases the results of both analyses agree with each other within the estimated theoretical uncertainty. Notice, however, that the EM

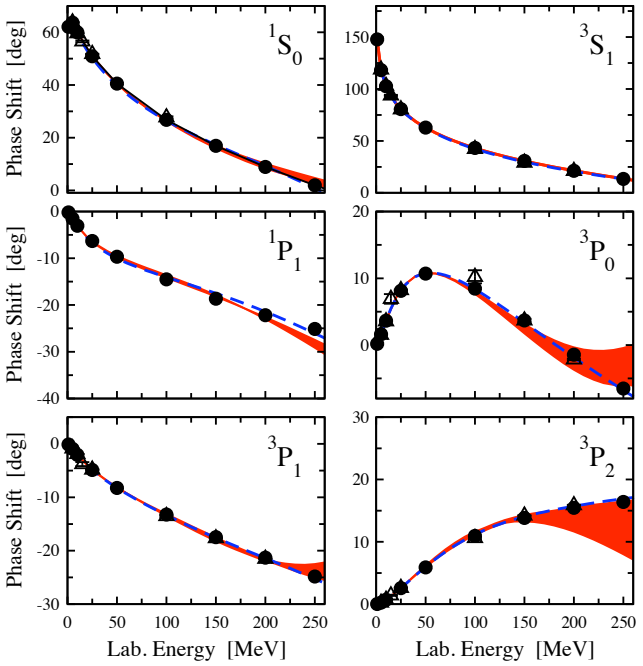

FIG. 15 Neutron-proton phase shifts in S- and P-waves at N^{3}LO in comparison with the Nijmegen (273; 274) (filled circles) and Virginia Tech (275) (open triangles) PWA. Shaded bands (dashed lines) refer to the calculations by EGM (272) (EM (271)).

[#6] Notice, however, that the value of the LEC c_4 adopted in (271), $c_4 = 5.4$ GeV^{-1} is not compatible with pion-nucleon scattering where one finds at order Q^3 (185): $c_4 = 3.40 \pm 0.04$ GeV^{-1}.

[#7] This number refers to isospin-invariant contact interactions.

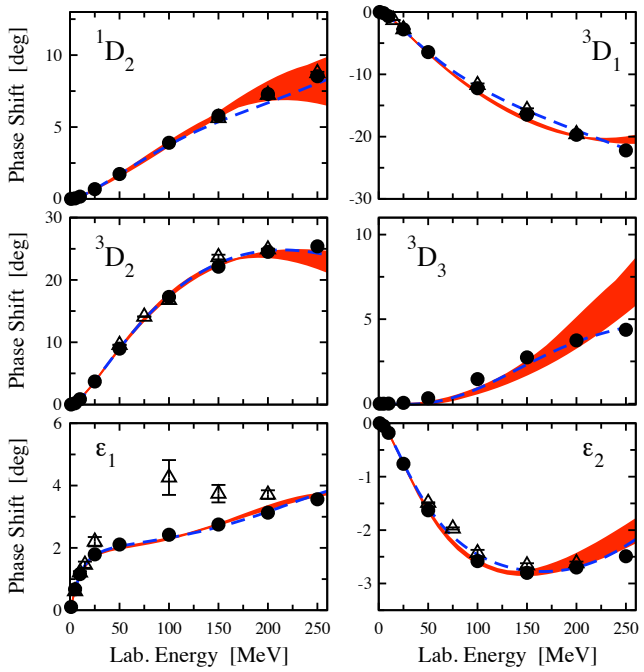

FIG. 16 Neutron-proton phase shifts in D-waves and the mixing angles $\epsilon_{1,2}$ at N^{3}LO. For notation see Fig. 15.

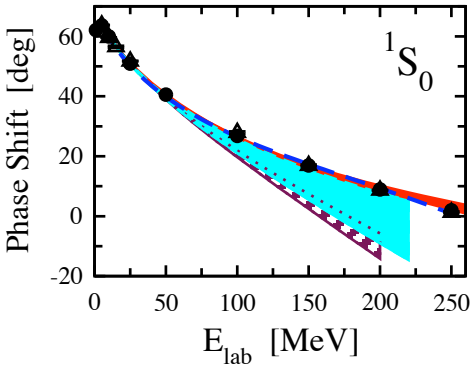

FIG. 17 Neutron-proton ^{1}S$_0$ partial wave at NLO (dashed band), N^{2}LO (light-shaded band) and N^{3}LO (dark-shaded band) in comparison with the Nijmegen (273; 274) (filled circles) and Virginia Tech (275) (open triangles) PWA.

and EGM analyses differ from each other in several important aspects. For example, the so-called spectral function regularization (155; 156) of the 2π-exchange contributions has been adopted by EGM while the analysis by EM is based upon dimensionally regularized expressions. Further differences can be attributed to the implementation of the momentum-space cutoff in the Schrödinger equation and the treatment of relativistic effects. More precisely, the work by EGM is based on the "relativistic" Schrödinger/Lippmann-Schwinger equation, a natural extension of the usual nonrelativistic equations utilizing the relativistic relation between the CMS energy and momentum, see (170) for more details. This equation can be straightforwardly generalized to the case of several nucleons, see (276–278) for recent studies of relativistic effects in 3N observables, and can also be cast into equivalent nonrelativistic-like forms (170; 279) (provided the potential is appropriately modified). On the other hand, the analysis of Ref. (271) is based on the nonrelativistic Schrödinger equation and uses the static 1π-exchange potential and the $1/m$- and $1/m^2$-corrections to the 2π-exchange potential from Refs. (142; 173), where no particular dynamical equation is specified. It is unclear whether the relativistic corrections to the potential used in (271) are consistent with the nonrelativistic Schrödinger equation. Further differences between the EGM and EM analyses result from the fitting procedure: the LECs accompanying the contact interactions were determined by EM/EGM by fitting directly to the scattering data/to the Nijmegen PWA (273; 274). For this reason, EGM adopted the same treatment of IB effects as followed by the Nijmegen group and did not include e.g. the leading IB contributions to the 2π-exchange potential. Perhaps, the most important difference between the two studies is related to the estimation of the theoretical uncertainty. In the work by EGM, the theoretical uncertainty was estimated by varying the cutoffs in the Schrödinger equation and the spectral function representation for the 2π-exchange potential restricted by the condition that the resulting LECs are of a natural size which might be viewed as a self-consistency check for calculations carried out within the power counting scheme based on naive dimensional analysis, see (87; 163). Notice further that at NLO and N^{2}LO, the strengths of various contact interactions are well understood in terms of resonance saturation on the basis of phenomenological one-boson exchange models (280). No serious attempt to provide a realistic error estimation was done in the analysis of EM. On the other hand, their work clearly demonstrates that for a particularly chosen regularization prescription it is even possible to accurately describe two-nucleon scattering data for $E_{\rm lab} > 200$ MeV. For further technical details, results for various scattering observables and the properties of the deuteron the reader is referred to the original publications (271; 272) and the review article (163).

To illustrate the convergence of the chiral expansion for NN phase shifts, we show in Fig. 17 the results for the $^1S_0$ partial wave at NLO, N^{2}LO (156) and N^{3}LO (272). We emphasize that the variation of the cutoff at both NLO and N^{2}LO only shows the effects of missing N^{3}LO contact interactions. It, therefore, does not provide a realistic estimation of the theoretical uncertainty at NLO, see (163) for an extended discussion.

Applications to the three-nucleon system have so far been carried out up to N^{2}LO. At NLO, no 3NF needs to be taken into account. This allowed for a parameter-free predictions of various 3N scattering observables at low energies as well as for the triton and α-particle binding energies (122). Using the most recent version of the

NLO potential based on the spectral functions regularization, one finds at NLO (163) $B_{^3\mathrm{H}} = 7.71 \ldots 8.46$ MeV and $B_{^3\mathrm{He}} = 24.38 \ldots 28.77$ MeV to be compared with the experimental values $B_{^3\mathrm{H}} = 8.482$ MeV and $B_{^3\mathrm{He}} = 28.30$ MeV. These numbers are similar to the ones obtained in Ref. (122) within the framework based on dimensional regularization.

At N^{2}LO one, for the first time, has to take into account the crresponding 3NFs. The two LECs D and E entering the expressions for the 3NF in Eq. (2.22) have been determined by fitting the ^{3}H binding energy and either the nd doublet scattering length (123), the ^{4}He binding energy (281) or the properties of light nuclei (282). Notice that the $\pi NNNN$ vertex entering the 1π-exchange-contact 3NF also plays an important role in processes with a completely different kinematics such as e.g. the pion production in the NN collisions (283), see section II.E, or weak reactions like $pp \to de^+\nu_e$, see (284) and references therein. This offers the possibility to extract the corresponding LEC from these processes, see (284) for a recent attempt. With the LECs being determined as described above, the resulting nuclear Hamiltonian can be used to describe the dynamics of few-nucleon systems. In particular, 3N continuum observables offer a natural and rich testing ground for the chiral forces. In Refs. (122; 123; 285–293) various 3N scattering observables have been explored by solving the momentum-space Faddeev equations with chiral two- and three-nuclein forces as input. In the formulation of Ref. (22), one first computes the T-matrix by solving the Faddeev-like integral equation

$$\begin{aligned} T &= t\,P\,\phi + (1 + t\,G_0)\,V_{3N}^1\,(1+P)\,\phi + t\,P\,G_0\,T \\ &+ (1 + t\,G_0)\,V_{3N}^1\,(1+P)\,G_0\,T\,, \end{aligned} \tag{2.38}$$

where the initial state ϕ is composed of a deuteron and a momentum eigenstate of the projectile nucleon. Here V_{3N}^i is that part of the 3N force which singles out the particle i and which is symmetric under the interchange of the two other particles. The complete 3NF is decomposed as $V_{3N} = V_{3N}^1 + V_{3N}^2 + V_{3N}^3$. Further, $G_0 = 1/(E - H_0)$ is the free propagator of the nucleons, P is a sum of a cyclical and anti-cyclical permutation of the three particles and t denotes the two-body t-matrix. Once T is calculated, the transition operators U_{el} and U_{br} for the elastic and break-up channels can be obtained via

$$\begin{aligned} U_{\mathrm{el}} &= P\,G_0^{-1} + P\,T + V_{3N}^1\,(1+P)\,(1+G_0\,T)\,, \\ U_{\mathrm{br}} &= (1+P)\,T\,. \end{aligned} \tag{2.39}$$

For details on solving these equations in momentum space using a partial wave decomposition the reader is referred to (294). The partial wave decomposition of the 1π-exchange and contact 3NF at N^{2}LO and the one-pion-two-pion-exchange topology at N^{3}LO is detailed in Refs. (123) and (295), respectively. The expressions for various observables in terms of the transition operators are given in (22). The inclusion of the long-range electromagnetic interaction requires a non-trivial generalization of the formalism, see (296; 297) for recent progress along this line.

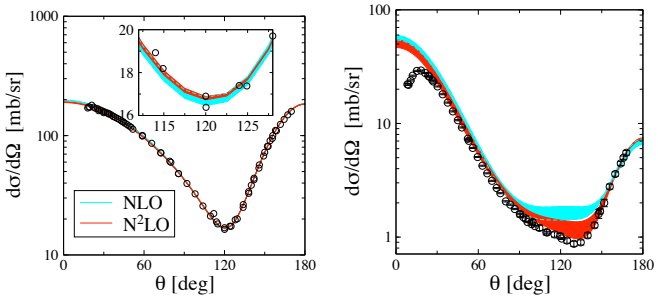

FIG. 18 Differential cross section for elastic nd scattering at $E_{\mathrm{lab}} = 10$ MeV (left panel) and 65 MeV (right panel). Light (dark) shaded bands depict the results at NLO (N^{2}LO). The neutron-deuteron data at 10 MeV are from Ref. (298). The remaining data at 10 MeV are the Coulomb/IB-corrected proton-deuteron data from Refs. (299–301). The data at 65 MeV are proton-deuteron data from Ref. (302).

The results for the differential cross section in elastic nd scattering are in a good agreement with the data, see Fig. 18 for two representative examples. Notice, however, that the theoretical uncertainty becomes significant already at intermediate energies. Qualitatively, this behavior is consistent with the one observed in the two-nucleon system (272). Notice further that the description of the data improves significantly when going from NLO to N^{2}LO. The situation is similar for vector and tensor analyzing powers, see Ref. (163) for a recent review article. More complicated spin observables have also been studied. As a representative example, we show in Fig. 19 a selection of the proton-to-proton and proton-to-deuteron polarization transfer coefficients measured in $d(\vec{p},\vec{p})d$ and $d(\vec{p},\vec{d})p$ reactions at $E_p^{\mathrm{lab}} = 22.7$ MeV (303; 304). The results at N^{2}LO are in a reasonable agreement with the data, see (302) for more examples. One further observes that the theoretical uncertainty obtained by the cutoff variation is underestimated at NLO, see the discussion earlier in the text. It is, however, comforting to see that the description of the data improves significantly when going from NLO to N^{2}LO.

The nucleon-deuteron breakup reaction offers even more possibilities than the elastic channel due to the much richer kinematics corresponding to three nucleons in the final state. It has also been studied extensively over the last years, both theoretically and experimentally, leaving one with mixed conclusions. While the differential cross section in some configurations such as e.g. the recently measured np final-state interaction, co-planar star and an intermediate-star geometries at low energies are in a very good agreement with the data (287), large deviations are observed in certain other configurations. In particular, the so-called symmetric space-star configuration (SST) appears rather puzzling. In this configuration, the plane in the CMS spanned by the outgoing nu-